



UNIVERSIDADE D
COIMBRA

Samuel José dos Reis Alves

**DESIGN AND MANUFACTURING OF SOFT
ROBOTICS MECHANISMS: IMPROVING THE
RELIABILITY OF PNEUMATIC-BASED
SOLUTIONS**

Dissertação no âmbito do Mestrado Integrado em Engenharia Mecânica, no ramo de produção e projeto orientada pelo Professor Doutor Pedro Mariano Simões Neto e apresentada ao Departamento de Engenharia Mecânica da Universidade de Coimbra.

Outubro de 2020

1 2



9 0

FACULDADE DE
CIÊNCIAS E TECNOLOGIA
UNIVERSIDADE DE
COIMBRA

Design and manufacturing of soft robotics mechanisms: improving the reliability of pneumatic-based solutions

Submitted in Partial Fulfilment of the Requirements for the Degree of Master in Mechanical Engineering in the speciality of Production and Project

Projeto e fabricação de mecanismos de *soft robotics*: melhorando a fiabilidade de soluções pneumáticas

Author

Samuel José dos Reis Alves

Advisor

Pedro Mariano Simões Neto

Jury

President **Professor Doutor José Luís Ferreira Afonso**
Professor Auxiliar da Universidade de Coimbra

Vowels **Professor Doutor Mohammad Safeea**
Professor Convidado da Universidade de Coimbra
Professor Doutor Paulo Joaquim Antunes Vaz
Professor Adjunto do Instituto Politécnico de Viseu

Advisor **Professor Doutor Pedro Mariano Simões Neto**
Professor Auxiliar da Universidade de Coimbra

Coimbra, October, 2020

“With regard to performance, commitment, effort, dedication, there is no middle ground. Or you do something very well or not at all”

Ayrton Senna

Aos meus pais.

ACKNOWLEDGEMENTS

Coming to the end of an important stage in my life, it is time to thank all those who have guided and helped me through these years. To thank them not only for my development as a student, but also as a person.

First of all, to Prof. Dr. Pedro Neto a sincere appreciation for the opportunity to work in his laboratory, to experience this area that fascinated me and led to the realization of my dissertation. I am grateful for his guidance, all the support and the constructive critics.

I am also grateful to teachers Diogo Neto and Nuno Mendes for all their advice and availability to enhance my work.

To my colleagues in the laboratory who work with great professionalism, always ready to help and with an incredible spirit of teamwork. Thank you for motivating me to follow the same path. To Pedro Matos, a former laboratory colleague and above all to a great friend.

To my parents, my sister and my brother-in-law, for being always by my side throughout the entire academic journey, for all the unconditional encouragement that contributed to my growth.

To all my friends that I have made during these five years and to those who have always supported me.

Finally, to a special person that is always pushing me and encouraging me to go further, I have no words to describe my enormous gratitude. Thank you for all that you have done for me, Mariana.

Abstract

Nowadays, robots are used in a wide range of applications such as industrial manufacturing, medical services and even in leisure applications. Robots have substantially increased their capabilities in terms of speed, precision and task execution abilities. However, they are commonly made of rigid materials, presenting limitations in terms of deformation and adaptation when handling fragile and/or complex objects, especially when the environment is not entirely known. These applications require a compliant robot behaviour both at software and hardware level. In order to deal with such a requirement, a new robotics subarea, called soft robotics, arises. This new subarea is based on biological structures and allows a designer to create robot components, with elastic, flexible and low rigidity materials (soft materials).

Soft robotics has proven its potential in the manufacture of grippers and manipulators. Soft materials provide the ability to create realistic shapes, reduced weight and increase the safety of the equipment. In this context, this dissertation presents the design and manufacture of a pneumatic robotic hand prototype made of soft materials, and partially fabricated by 3D printing. This concept allows the design and fabrication of an anthropomorphic hand at a low cost, with anatomical shape, desired compliance and reduced control complexity (since the number of actuated degrees-of-freedom is lower than the number of degrees-of-freedom of the robotic hand).

There is no systematic procedure or methodology to simulate the behaviour of elastic materials. A numerical model implemented in Finite Element Analysis (FEA) is proposed to simulate the hand behaviour when it is actuated. Simulations results proved the model effectiveness when compared with experimental tests.

Keywords Compliance, Soft robotics, Soft materials, Pneumatic robotic hand, 3D printing, FEA.

Resumo

Atualmente, os robôs operam em diversos tipos de indústria, serviços médicos e até mesmo em aplicações de lazer. Os robôs têm melhorado as suas características ao nível da velocidade, precisão e capacidade de repetição de tarefas. Contudo, os mecanismos robóticos tradicionais são normalmente constituídos por materiais rígidos, apresentando dificuldades de deformação e adaptação, principalmente no manuseamento de objetos frágeis e/ou complexos, assim como em aplicações onde o ambiente não é perfeitamente conhecido. Estas aplicações requerem um comportamento robótico complacente, tanto ao nível de software como de hardware. Assim, surge uma nova subárea da robótica, chamada *soft robotics*. Baseando-se em estruturas biológicas, esta assenta no desenvolvimento de componentes robóticos com materiais elásticos, flexíveis e de baixa rigidez (materiais suaves).

Esta subárea comprovou apresentar potencial significativo na fabricação de *grippers* e manipuladores. A possibilidade de fabricar estruturas de materiais suaves, permite criar formas realísticas, diminuir o peso, lidar com um vasto número de objetos e aumentar a segurança dos equipamentos. Neste âmbito, esta dissertação apresenta o *design* e o processo de fabricação de um protótipo de uma mão robótica, atuada pneumáticamente, concebida com materiais suaves, parcialmente fabricados pelo processo de impressão 3D. Este conceito permite o desenvolvimento de uma mão robótica a um custo relativamente reduzido, com forma anatómica e reduzida complexidade de controlo.

O estudo do comportamento dos materiais elásticos é também estudado nesta dissertação. É proposto um modelo numérico, utilizado na Análise de Elementos Finitos (FEA) para simular o comportamento da mão quando esta está atuada. Os resultados das simulações são comparados com testes experimentais, comprovando assim parcialmente a viabilidade do modelo numérico.

Palavras-chave: Conformidade, *Soft robotics*, Materiais suaves, Mão robótica pneumática, Impressão 3D, FEA.

Contents

LIST OF FIGURES	ix
LIST OF TABLES	xiii
LIST OF SYMBOLS AND ACRONYMS	xv
List of Symbols.....	xv
Acronyms	xv
1. Introduction	1
1.1. Problem and Motivation	2
1.1.1. Grasping and Manipulation	2
1.1.2. Soft Robots Limitations.....	2
1.2. Proposed Approach.....	3
1.3. Thesis Overview	3
2. State of the art.....	5
2.1. Types of Actuators.....	7
2.2. Manipulators and Grippers	9
2.3. Soft Robotics Hands	13
2.4. Soft Robots Manufacturing.....	15
2.5. Finite Element Analysis.....	18
3. Soft Robotics Hand Concept	21
3.1. Human Hand Anatomy	21
3.1.1. Bones and Joints	21
3.1.2. Actuation Strategies.....	23
3.2. System Requirements	24
3.3. Manufacturing.....	25
3.3.1. Materials	26
4. Design and Implementation.....	31
4.1. Finger	31
4.1.1. Dimensions	31
4.1.2. Manufacturing	31
4.1.3. Testing and Results.....	33
4.2. Hand.....	33
4.2.1. Hand Design	33
4.2.2. Manufacturing	34
4.2.3. Testing and Results.....	39
5. Numerical Modelling of the Finger Fold.....	41
5.1. Non-linear Analysis and Hyperelastic Materials	41
5.2. Development of the Computational Model	44
5.2.1. Exoskeleton	45
5.2.2. Fibre-Reinforced Actuator.....	50
5.2.3. Assembly - (Exoskeleton and Fibre-Reinforced Actuator).....	56

- 5.2.4. Finger Force Test 61
- 6. Conclusions 63
 - 6.1. Future Work..... 64
- BIBLIOGRAPHY 67
- Appendix A (Finger dimensions)..... 71
- Appendix B (Printing parameters) 72
- Appendix C (Ecoflex™ Series – Technical bulletin)..... 73
- Appendix D (Filaflex 82A – Technical bulletin) 75
- Appendix E (Ninjaflex – Technical bulletin)..... 76

LIST OF FIGURES

Figure 2.1. Robot structure example: (a) Discrete; (b) Continuous [5].....	5
Figure 2.2. Biological inspiration. (a) Octopus arm; (b) Scheme of the muscle arrangement of the octopus arm [4].	6
Figure 2.3. Examples of hydrostatic muscles. (a) The elephant trunk; (b) The arms and tentacles of squid; (c) The dog tongue [1].....	6
Figure 2.4. Octopus robot arm with cables and SMAs springs [4].	7
Figure 2.5. Three types of fluidic elastomer actuators. (a) Pleated; (b) Ribbed; (c) Cylindrical; (1) unactuated state; (2) actuated state [9].	7
Figure 2.6. Granular jamming concept – (a),(b) [2]; Passive particle jamming concept – (c),(d) [15], [14].....	9
Figure 2.7. Soft surgical manipulator. (a) One fibre-reinforced actuator pressurized; (b) Internal design. (FFA – flexible fluidic actuator) [16].....	10
Figure 2.8. Soft robotics grippers based on pleated actuator concept. (a) Soft robotics finger [5]; (b) Orange picking test [5]; (c) Soft gripper grasping a paper container with food materials [19]	11
Figure 2.9. Grippers with different fingers arrangements. (a) Five fingers; (b) Four fingers; (c) Inspired by the human hand [21].	12
Figure 2.10. A fabric-based lightweight robotic gripper with two fingers [23].	12
Figure 2.11. Soft gripper based on Fin Ray® Effect. (a) MultiChoiceGripper; (b) Adaptive gripper DHDG.....	13
Figure 2.12. Three different concepts of soft robotics hands. (a) Soft robotics glove [28]; (b) Soft prosthetic hand via stretchable optical waveguides [29]; (c) The RBO Hand 2 [6].....	14
Figure 2.13. Soft pneumatic prosthetic hand. (a) Grasping a lamp [3]; (b) Grasping a pen [30].	15
Figure 2.14. Soft lithography fabrication process for soft fluidic elastomer robots [9].	15
Figure 2.15. Three types of additive manufacturing (AM). (a) Fused deposition modelling (FDM); (b) PolyJet; (c) Stereolithography (SLA).....	16
Figure 2.16. 3D printing with Ninjaflex material [33]. (a) Printed actuator; (b) A high force soft gripper; (c) Soft robotics hand exoskeleton to assist finger flexion.....	17
Figure 2.17. Direct ink writing scheme (DIW) [32].....	17
Figure 2.18. 3D printed soft robots based on DIW. (a) 4 channel tentacle; (b) Quadrupedal robot; (c) Pneu-net actuator.....	18

Figure 3.1. Bones and Joints of the Human Hand (left hand). CMC – Carpometacarpal, MCP – Metacarpophalangeal, IP – Interphalangeal, PIP – Proximal Interphalangeal, DIP – Distal Interphalangeal joints [39].	22
Figure 3.2. The motion of each joint; (a), (b) and (c) – Flexion, extension and abduction/adduction of the MCP joint, respectively; (d) and (e) – Flexion of the PIP and DIP joint, respectively [39].	22
Figure 3.3. Thumb Movement Types [41].	23
Figure 3.4. Concept of the soft hand fingers. (a) Fibre-reinforced actuator; (b) Finger exoskeleton; (c) Opposition/reposition thumb actuators.	25
Figure 3.5. Shore hardness scales of SmoothOn, Inc.	28
Figure 3.6. TPE formation diagram.	28
Figure 4.1. Finger exoskeleton made with Filaflex 82A material. (a) Top view; (b) Front view.	31
Figure 4.2. PLA printed parts. (a) Mould assembly with the largest core; (b) and (c) Mould parts; (d) Largest core; (e) Smaller core.	32
Figure 4.3. Fibre-reinforced actuator.	32
Figure 4.4. Assembly of the finger exoskeleton and the fibre-reinforced actuator.	33
Figure 4.5. Hand exoskeleton. (a) Back side; (b) Palm side.	34
Figure 4.6. Polyethylene terephthalate thread.	35
Figure 4.7. 3D printing parts for the construction of the actuators. (a) to (f) mould parts; (g) and (h) actuator parts.	35
Figure 4.8. Silicone rubber Ecoflex™ 00-50.	36
Figure 4.9. Preparation of Ecoflex™ 00-50 before casting.	37
Figure 4.10. Mould concept used in the construction of the actuators.	38
Figure 4.11. Fibre-reinforced index actuator.	39
Figure 4.12. Soft pneumatic hand. (a) Isometric view; (b) Front view.	40
Figure 5.1. A typical stress-strain curve of a metallic material. Linear and Non-linear areas.	41
Figure 5.2. Different material behaviours. Visualization of the stress-strain curve for: Linear, Nonlinear Elastic, Bi-Linear Elasto-plastic, Plastic and Hyperelastic materials.	42
Figure 5.3. Simplification of the model. (a) Hand design with visualization of the plans to cut off the finger - CAD file; (b) Index finger exoskeleton - CAD file.	45
Figure 5.4. Modelling of index finger exoskeleton in <i>Autodesk Inventor Nastran</i> ®. Fixed constraint, applied force and gravity.	47
Figure 5.5. Vertical displacement for each force applied. Comparison of experimental tests and 3 different types of FEM (MR set 1, MR set 2 and MR set 3.)	48

Figure 5.6. Vertical displacements of the index finger exoskeleton and the maximum deflection value from the tip of the finger to the bottom surface of the hand (degrees). All displacements values in mm. Left-side: experimental tests and right-side: FEM - MR set 3 with the results in von Mises Stress [MPa]. Forced applied: (a) Own weight (b) 0.07 N (c) 0.16 N (d) 0.27 N (e) 0.40 N (f) 0.56 N.	49
Figure 5.7. Pressurized actuator modelling without reinforcement (a) and with reinforcement (b). Both models pressurized with 30 kPa. Von Mises Strain results.	50
Figure 5.8. First simplification. Real vs Numerical PET reinforcement geometry. (a) Cylindrical cross-section with 0,25 mm diameter; (b) Square cross-section with 0,5 mm width (44 rings).	52
Figure 5.9. Second simplification. (a) Illustration of the exoskeleton hole area; (b) Experimental actuator base; (c) FEM actuator base.	52
Figure 5.10. FEM Model development. 1 – Fixed constraint; 2 – Half-symmetric constraint; 3 – Internal pressure.	53
Figure 5.11. Horizontal displacement for each force applied. Comparison of experimental tests and 3 different types of FEM (Ogden set 1, Ogden set 2 and Ogden set 3).	54
Figure 5.12. Fibre-reinforced actuator test. Left-side: experimental tests (EXP2) and right-side: FEM simulations with von Mises Strain results (FEM- Ogden set 3). (a) 20 kPa; (b) 40 kPa; (c) 50 kPa; (d) 60 kPa.	55
Figure 5.13. Experimental results of the index finger. Vertical displacement results of EXP3. All displacements are in mm.	56
Figure 5.14. FEM model development. 1 – Fixed constraint; 2 – Ty constraint; 3 – Half-symmetric constraint; 4 – Internal pressure.	57
Figure 5.15. Contact surfaces between the exoskeleton and the actuator. (1), (4), (6), (8), (9), (10) – Sliding/no separation; (2), (3), (5), (7) – Separation.	58
Figure 5.16. FEM simulation of a fibre-reinforced actuator with D=10. (20 kPa)	59
Figure 5.17. FEM results of the assembly (Exoskeleton + Fibre-reinforced actuator). Visualization of von Mises Strain results, vertical displacement and folding angle. All displacement values are in mm.(a) 20 kPa; (b) 30 kPa; (c) 40 kPa; (d) 47 kPa.	60
Figure 5.18. Vertical displacement for each pressure applied. Comparison between experimental tests and FEM simulations	60
Figure 5.19. Determination of the maximum fingertip force. (a) Experimental test for 60 kPa; (b) FEM simulation for 46,5 kPa.	62
Figure 5.20. EXP and FEM results of maximum fingertip pressure force.	62
Figure A.1. Nomenclature of dimensions.	71

LIST OF TABLES

Table 3.1. Technical overview of three platinum-catalysed silicone types.....	27
Table 3.2 Technical overview of three TPE materials.	29
Table 5.1. Different models to characterize hyperelastic materials: Neo-Hookean, Ogden, Yeoh and Mooney-Rivlin[48],[33].....	42
Table 5.2. Parameter values of different hyperelastic models to characterize Ecoflex™ 00-30, Ecoflex™ 00-50 and Dragon Skin™ 30 materials [49].....	43
Table 5.3. Parameter values of different hyperelastic models to characterize Ninjaflex material [33].	44
Table 5.4. Measurements of the maximum vertical displacements of the index finger obtained experimentally when subjected to: own weight, 7 g, 16 g, 28 g, 41 g and 57 g.	46
Table 5.5. Set of parameters of the Ninjaflex Mooney-Rivlin model. MR set 1 – Taken from the article [33]. MR Set 2 and 3 – Implemented adjustments.	47
Table 5.6. Results of maximum horizontal displacement for the respective pressures. Three experimental tests and the average for each pressure.....	51
Table 5.7. Ogden parameter values for Ecoflex™ 00-50. FEM-Ogden set 1 – parameters obtained for bibliographic review. FEM Ogden set 2 and 3 – improvements to achieve a characterization closer to the experimental.	51
Table 5.8. Results of maximum vertical displacement for the respective pressures. Three experimental tests and the average for each pressure.....	56
Table A.1. Exoskeleton finger dimensions.....	71
Table A.2. Fibre-reinforced actuators dimensions.	71
Table B.1. Printing parameters.	72

LIST OF SYMBOLS AND ACRONYMS

List of Symbols

E – Modulus of Elasticity

σ_s – Ultimate Tensile strength

σ_y – Yield strength

ρ – Mass density

m – Weight

V – Volume

Acronyms

3D – Three-dimensional

ABS – Acrylonitrile butadiene styrene

AM – Additive manufacturing

CAD – Computer-Aided Design

CMC – Carpometacarpal

DID – Distal Interphalangeal

DIW – Direct ink writing

DOF – Degrees-of-Freedom

EAP – Electroactive polymers

EXP – Experimental

FDM – Fused Deposition Modelling

FEA – Finite Element Analysis

FEM – Finite Element Method

IP – Interphalangeal

MIS – Minimally invasive surgery

MCP – Metacarpophalangeal

PET – Polyethylene Terephthalate

PIP – Proximal Interphalangeal
PLA – Polylactic acid
PWM – Pulse width modulation
SMA – Shape Memory Alloy
SLA – Stereolithography
STL – Stereolithographic Format
TPE – Thermoplastic Elastomers

1. INTRODUCTION

Robots are increasingly used in different areas providing outstanding characteristics such as speed, accuracy, controllability of repetitive tasks and load capacity. However, they are made with rigid and heavy materials, and, thus, they cannot adapt or deform their shape when they encounter an obstacle, limiting the ability to interact with the environment, especially with humans. Furthermore, traditional robots have limitations when they need to handle fragile or complex objects due to the lack of flexibility and dexterity [1][2][3].

To overcome such problems, researches inspired in nature are being made in order to understand the movement and manipulation capabilities of some animals and plants that have both, a soft body and can reproduce excellent handling tasks. There are many examples such as elephant trunk, octopus arm, worm and lizard, that are sources of inspiration to improve the limitations of the conventional robots [1][4].

In this context, the robotics subfield called Soft robotics was born, which consists of creating components made of materials with compliance similar to soft biological materials, allowing to increase flexibility and adaptability, as well as improving safety when in contact with the environment. Additionally, soft robots have simple control systems and structures, that can be built using relatively low-cost materials.

1.1. Problem and Motivation

1.1.1. Grasping and Manipulation

The concept of grasping and manipulation differs according to what each entity needs to perform. Thus, it is common for industrial robots to have specialized grippers only for the objects which they have to deal with, in order to maximize their own production. However, if the applicability of a robot has to change from an environment with fixed tasks to an environment with variable tasks, such as handling objects with different sizes, shapes, materials, surfaces and fragility levels, it is more challenging to find tools capable of responding effectively. Concerning manipulation, it is the ability to move the grasped objects at different speeds and trajectories. A correct grasping will usually conduct a successful manipulation task.

During the last few years, the robotic community have been developing many applications of soft robots as grippers and manipulators, being that soft robots have a great potential, when it comes to grasping fragile objects that currently are a great limitation for "hard grippers".

The human hand has been the focus of many research activities, as a result of excellent combinations of characteristics that allow handling any object efficiently. Currently, there are already many robotic hands that have excellent skills and sophisticated mechanisms. Nevertheless, these robotic hands present complex systems, rigid structures and high investments. Therefore, soft robotics hands have been created combining rigid and soft structures, or even just soft structures.

1.1.2. Soft Robots Limitations

Despite the various advantages of soft robotics, this field is relatively new, and a lot of research and experimentation is needed to make better use of them. As research progresses, new milestones are achieved, and new limitations arise.

Most of the grippers created based on this approach can only pick up lighter objects due to the low forces that they can execute. This presents many limitations when it is necessary to deal with several different objects.

Regarding the structural integrity and manufacturing of soft mechanisms, most soft grippers are made of material casting (mixing two components to cure) with a 3D printed

mould. This process requires manual skills, time, and some care due to the great possibility of the appearance of defects, such as pores (based on trial and error system). Moreover, most soft mechanisms are neither structurally analysed nor optimised in their geometry, so Finite Element Analysis (FEA) can be a great help once it allows the prediction of experimental results, allowing faster improvements, saving resources and time. Some researchers already use this tool, but it is not yet frequent.

1.2. Proposed Approach

The proposed approach consists of designing and manufacturing a soft robotics hand (pneumatically actuated), with the aim of improving conventional robotic hands. The development of this hand will consider the current limitations of soft robots, focusing on their resolution.

According to the necessity to obtain more load capacity to pick up heavier objects, a thermoplastic elastomer (TPE) will compose one of the components of the hand. These types of flexible materials have more rigidity compared to silicones that are commonly used.

Additionally, to facilitate the manufacturing and to decrease the time of the process, to increase production efficiency and to improve mechanical properties, the main structure of the hand will be printed directly from a 3D printer with flexible material filaments (from CAD to production).

Finally, in order to analyse and improve the design of the developed human hand mechanism, a finite element model (FEM) was developed using the *Autodesk Inventor Nastran*® software. The finger motion is numerically studied, allowing to compare the numerical results with the experimental ones.

1.3. Thesis Overview

This dissertation is composed of six chapters, starting with the introduction of the subject, the current limitations and the description of the proposed approach. The second chapter represents state of the art with the latest developments of soft robotics field.

The third chapter describes the required concepts for creating a soft robotics hand, introducing the main bone structures and joints of the hand; the system requirements used based on the bibliographic review; the materials chosen and the manufacturing processes. The fourth chapter refers to the application of the concepts mentioned, presenting the design and development of the soft robotics hand, going through the entire process of manufacturing and the assembly.

The fifth chapter is about the application of *Autodesk Inventor Nastran*® software to perform FEA simulations on the index finger of the hand. The study consists in predicting the folding behaviour of the finger when pressurized.

Finally, the last chapter presents the main results obtained and some suggestions for future work that can improve the prototype developed.

2. STATE OF THE ART

The robot structure can be classified according to the number of degrees-of-freedom (DOF), as discrete or continuous. In general, rigid robots have several flexible joints connected by stiff links. Each joint provides a rotation or a translation, corresponding to a degree of freedom of robot motion. The higher the number of DOF, the greater flexibility of the robot. In soft robots, there are no rigid links causing a continuous deformation distribution, or in other words, the number of DOF is infinite [1]. Thus, when the number of DOF is finite, the robot has a discrete structure, Figure 2.1(a), and, when the number of DOF is infinite, the robot has a continuous structure, Figure 2.1(b) [5].

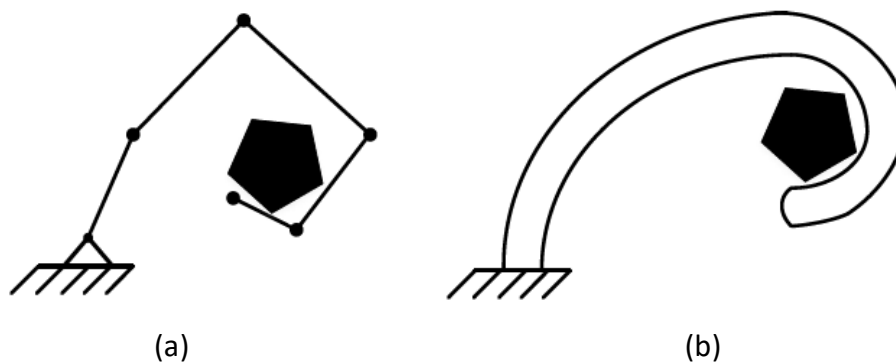


Figure 2.1. Robot structure example: (a) Discrete; (b) Continuous [5].

Rigid robots need an actuator for each stiff link to achieve the desired movements, that usually corresponds to an electric motor. In contrast, soft robots have integrated actuators and are distributed throughout the structure, and in many cases, they can occupy most of the structure or even the actuator can be the structure itself. This concept is designated “underactuated” because due to passive compliance of soft materials, the number of DOF is much higher than the number of degrees of actuation [6].

There are many examples of animals that have a soft body. The understanding of the morphology and functionalities of the structures of these animals allows learning new concepts that can be useful in soft robotics. Apparently, all animals with a soft body have a totally malleable body, although some animals as a snake or a lizard, have rigid elements with a large number of joints (high number of DOF). However, most of the soft robotics

studies focus on animals without rigid elements, such as the octopus, that has only hydrostatic muscles (infinite DOF) (Figure 2.2(a)).

The octopus is one of the first examples of inspiration in this area because it has eight arms composed of hydrostatic muscles, which provide excellent adaptation, deformation, locomotion and grasping skills towards his environment. Each arm is composed of three types of muscles groups: longitudinal, transversal and oblique, changing the length of the arm, bending in all directions and twisting (Figure 2.2 (b)).



Figure 2.2. Biological inspiration. (a) Octopus arm; (b) Scheme of the muscle arrangement of the octopus arm [4].

The elongation of the arm occurs according to the contraction of the transverse muscles (T), that is when the diameter of the muscle decreases and consequently, the length increases. Bending happens when the longitudinal muscles (L) on the one side of the arm are contracted, and after that, the transverse muscles are too. The twist results from the contraction of the oblique muscles (O). Furthermore, the arrangement of these muscles allows combined contractions, varying the stiffness of the arms and achieved high values of force [4]. Other examples of hydrostatic muscles are the elephant trunk (Figure 2.3(a)), the arms and tentacles of the squid (Figure 2.3(b)), and the dog tongue (Figure 2.3(c)). [1]

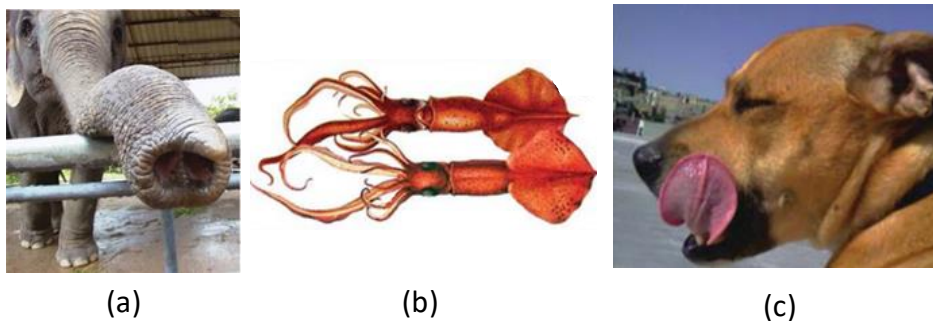


Figure 2.3. Examples of hydrostatic muscles. (a) The elephant trunk; (b) The arms and tentacles of squid; (c) The dog tongue [1].

2.1. Types of Actuators

Soft robots are commonly actuated by variable-length tendons or pneumatic/hydraulic actuation. In the first case, the variation occurs in the form of tension cables or shape-memory alloy actuators (SMA)[7]. Based on this approach, a prototype of a robotic octopus arm was made, with the actuation obtained through cables (longitudinally) and SMAs springs (transversely)[4].



Figure 2.4. Octopus robot arm with cables and SMAs springs [4].

In the second case, the pneumatic actuation consists of inflating channels in soft materials causing the desired deformations. Within this type of actuation, many actuators have been developed. Pneumatic artificial muscles, also known as McKibben actuators, were developed in the 1950s and 1960s to develop artificial muscles [8]. These muscles contain a flexible elastomer tube with reinforcement of braided fibres, being closed at the ends. The fibre arrangement is placed so that, when the actuator is pressurized, transverse expansion and longitudinal contraction occur (volume conservation). Another type is the fluidic elastomer actuator, an actuator made of low hardness rubber and driven by a relatively low-pressure fluid. It can be divided into three types according to their geometry: pleated, ribbed and cylindrical [9].

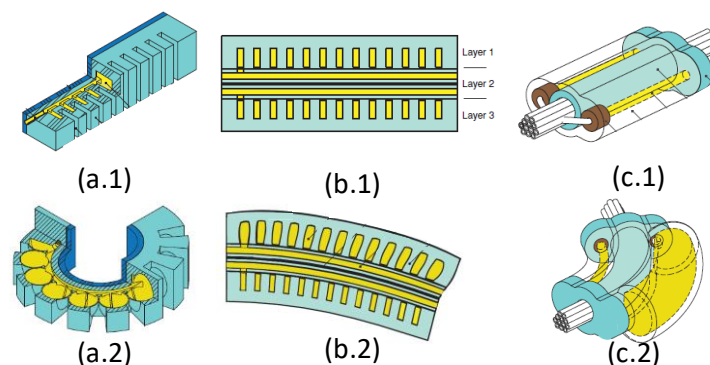


Figure 2.5. Three types of fluidic elastomer actuators. (a) Pleated; (b) Ribbed; (c) Cylindrical; (1) unactuated state; (2) actuated state [9].

The pleated actuator design consists in two parts: 1) the main body which expands when inflated; 2) a base containing the inextensible layer embedded in elastomer, that can be a paper, plastic, cloth or even stiffer rubbers. The main body is composed of discrete sections, which are separated by gaps. Each section has a chamber connected to a centre channel, and when is pressurized, all chambers are individually expanded. As one of the layers is inextensible, restricts axial deformation and favours the bending of the actuator (Figure 2.5(a)). The pleated actuator is also designated as pneumatic networks [10]. The ribbed actuator provides bidirectional bending, being composed by two fluidic elastomer actuators separated through an inextensible constrain layer. Each actuator is similar to the pleated actuator, but with ribs placed between channels (Figure 2.5(b)). The cylindrical actuator has the same principle of a ribbed actuator, but with a different morphology. The two actuators with several rectangular channels are substituted by two cylindrical actuators with only a cylindrical channel, and the constraining layer is replaced by a hollow core with stiffer silicone (Figure 2.5(c)).

To improve the desired motion of the actuators and to avoid unwanted deformations, some experiments introduced the concept of fibre-reinforced soft actuators [11],[12],[13]. It consists of wrapping the actuator with inextensible fibre, which will constrain it to radial swelling and restrict it to expand only in the longitudinal direction. Changing the fibre configuration allows the desired motions to be programmed mechanically. The chamber cross-section geometry and the density of the fibres along the length were analysed [13]. Furthermore, with the addition of fibre reinforcement, the actuators can withstand higher air pressures.

One of the soft technology disadvantages is the downforce to pick up objects, lack of stability and difficult in position control. To overcome this problem, some researchers suggest a variable stiffness of the actuators. In [2],[14],[15] is presented a concept referred to granular jamming, based on the placement of particles or grains inside the actuators and an external vacuum pump. In the normal state, the actuator is flexible, and when the structure is pumped out, the particles compress, and the actuator becomes rigid (Figure 2.6 (a), (b)). Another method is a passive particle jamming [14], that does not need vacuum pressure. A thin membrane with particles is placed over an actuator, as shown in Figure 2.6(d). When the actuator is expanded, the particles are passively jammed, increasing the stiffness. However, the compliance is affected by the particle membrane, which decrease the range

bending of the actuator. For this reason, it was created another actuator, developing the distributed particle sac with solid glass beads (Figure 2.6(c)). Moreover, as the mould manufacturing processes required many steps, becoming complex and time-consuming, the actuator was directly printed on a 3D printer (Makerbot Replicator 2X 3D) with Ninjaflex material [15].

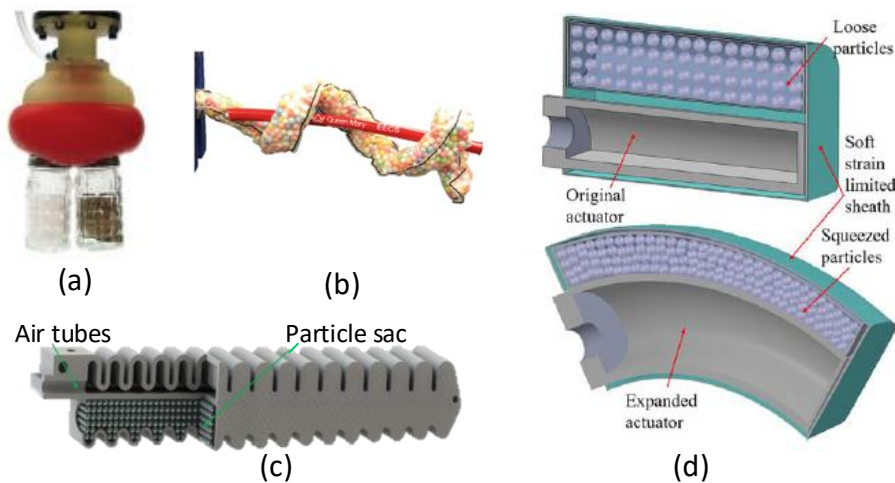


Figure 2.6. Granular jamming concept – (a),(b) [2]; Passive particle jamming concept – (c),(d) [15], [14].

In addition to the types of actuators mentioned, many researchers have focused on soft actuators composed of electroactive polymers (EAP), whose main characteristic is the change of the size or shape when an electric field stimulates them. There are several different types, such as dielectric EAP, ferroelectric polymers, electrostrictive graft polymers, liquid crystal polymers, ionic EAP, electrorheological fluids, ionic polymer-metal composites, and stimuli-responsive gels [7].

2.2. Manipulators and Grippers

In the medical field, minimally invasive surgery (MIS) is one of the most studied surgical operations, presenting great advantages relative to traditional open surgery as pain reduction, less bleeding and infection, and faster healing. However, rigid manipulators have a limited DOF movement being difficult to control them in small spaces, which can cause some damages to the human organism. These drawbacks led to the creation of a soft manipulator, which is composed of three fibre-reinforced actuators inside a soft body (Figure 2.7) [16]. The movements are created according to the pressurization of the actuators that

are equally distributed. Other examples of application to the same purpose are reported in [17] and [18].

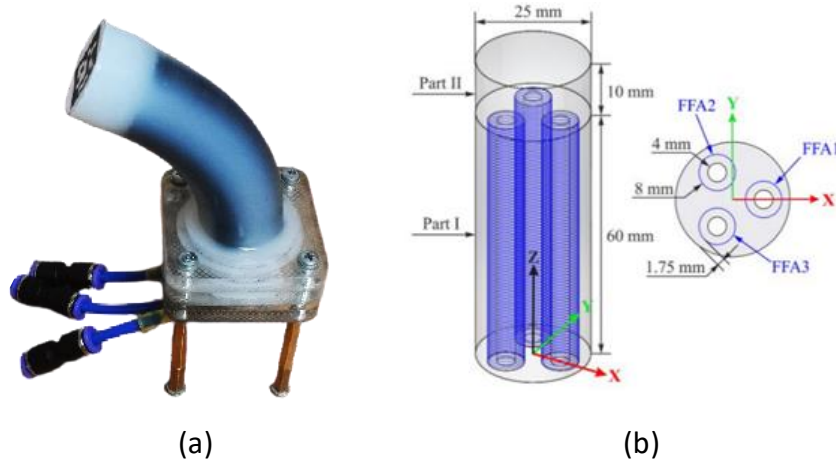


Figure 2.7. Soft surgical manipulator. (a) One fibre-reinforced actuator pressurized; (b) Internal design. (FFA – flexible fluidic actuator) [16].

During the 2018-2019 school year, based on the pleated actuator, it was developed in the Mechanical Engineering Department of the University of Coimbra, two soft robotics fingers for a collaborative gripper [5]. Each finger has a rigid part that was made with polylactic acid (PLA) material using a 3D printer, and an actuator made of a silicone rubber (Ecoflex™ 00-30) into a mould which was also produced on a 3D printer (Figure 2.8(a), (b)). The soft robotics fingers achieved good capacity to conform the fingers to the object's surfaces and pick-up objects. However, some problems occurred when the soft fingers were used to lift heavier objects. That happened because when more pressure was needed to inflate the fingers, air bubbles appeared due to the low thickness of the fingers. Similar work was developed in [19],[20] for studying grasping and lifting a paper container with food materials. The gripper is composed of three fingers made directly from the 3D printer (Object260connex) with a soft rubber-like (TangoBlack +).

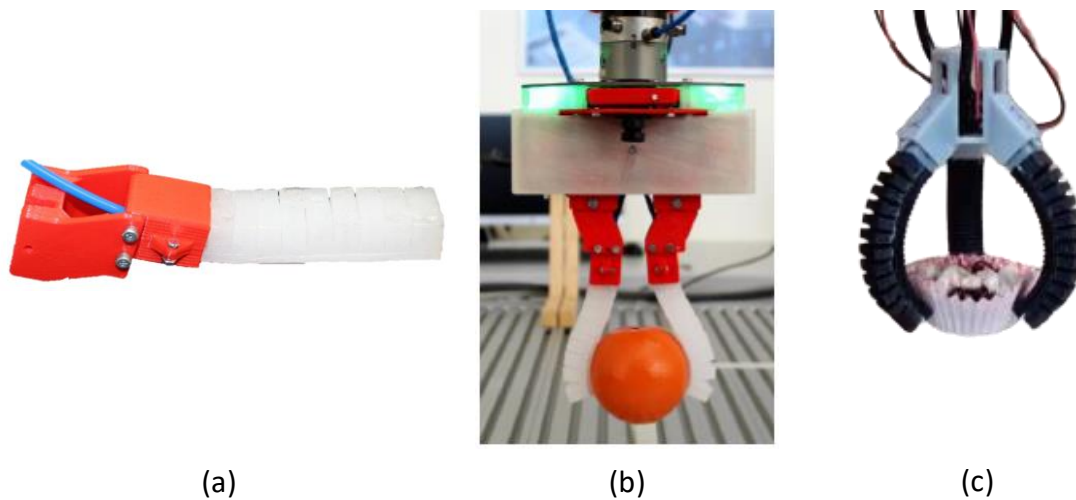


Figure 2.8. Soft robotics grippers based on pleated actuator concept. (a) Soft robotics finger [5]; (b) Orange picking test [5]; (c) Soft gripper grasping a paper container with food materials [19]

J.Fras et al. presents a soft flexible gripper design with different patterns of the finger's arrangements (Figure 2.9) [21]. The fingers are pneumatic actuators with a cylindrical cross-section, and two silicone layers constitute them with a reinforcement polyester thread in the middle acting as a reinforcement. The inner layer is made of a softer material (Ecoflex™00 - 50), while the outer layer is made of two silicones. The inner finger's side (grabbing part) is constituted by a stiffer silicone (SmoothSil 950), and the outer finger's side by the same material of the first layer. This combination provides the folding motion, which increases the grasping capabilities. The connection of all fingers is also made with Ecoflex™00 - 50. For a single finger, the bending angles as a function of the pressure exerted were analysed and then compared with a proposed mathematical model. The forces generated according to the pressure exerted by a finger with different lengths were also analysed, and different gripping capabilities were experienced for a five-finger arrangement. Similarly, a gripper with four fibre-reinforcement pneumatically actuators is presented in [22].

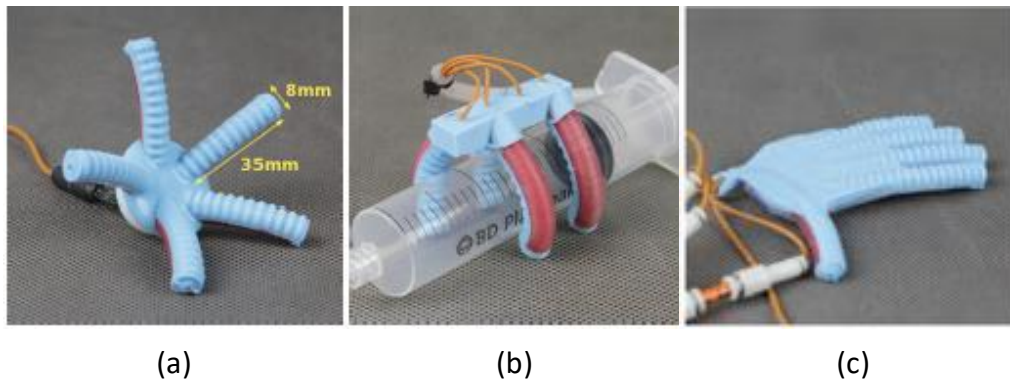


Figure 2.9. Grippers with different fingers arrangements. (a) Five fingers; (b) Four fingers; (c) Inspired by the human hand [21].

A fabric-based lightweight robotic gripper [23] is actuated by pneumatic pressure. The fingers are made of an airtight fabric with a pleated structure on one side of the finger. During pressurization, the pleats unfold while on the other side remains with the same length, causing deformation of the finger.

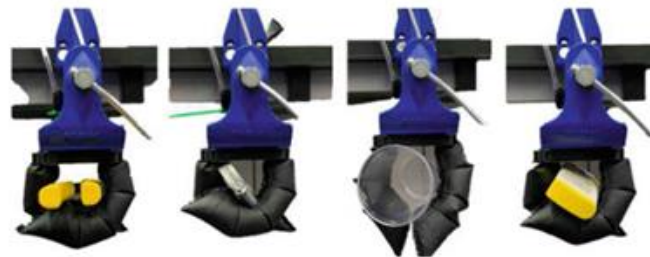


Figure 2.10. A fabric-based lightweight robotic gripper with two fingers [23].

A different gripper without actuation of soft components, but with interesting features, is the Fin Ray® Effect discovered by biologist Leif Kniese of Evologics GmbH, which is inspired by the physiology of fish fins [24]. The gripper fingers have a triangular structure with crossbeams that deform when pressed in opposition to the object, reaching the necessary compliance to pick up the object. The great results of this investigation led to the application of this methodology in Festo's grippers, such as MultiChoiceGripper [25] and the adaptive gripper DHDG [26]. In addition, some improvements have been made to create desired bending directions in order to require less force to obtain good adhesions on an object [27].

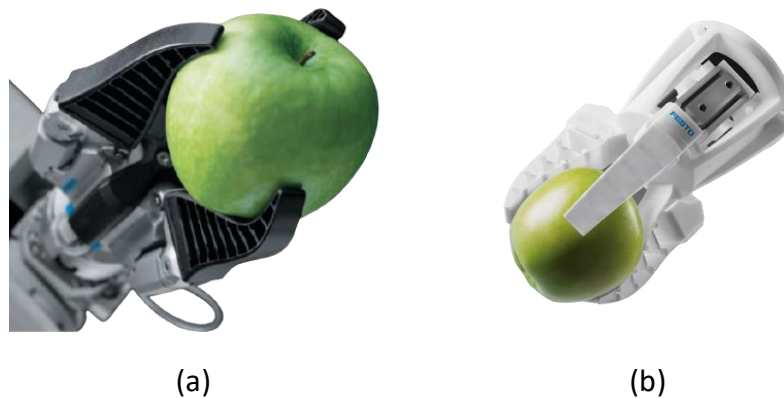


Figure 2.11. Soft gripper based on Fin Ray® Effect. (a) MultiChoiceGripper; (b) Adaptive gripper DHDG.

2.3. Soft Robotics Hands

The experiments with soft grippers motivated the development of soft pneumatic hands. The possibility to create an anatomical shape hand and the same time with characteristics of existing robotic hands made of rigid structures has been researched and experienced.

In this way, some examples of soft robotics hands have been presented. Firstly, it is not exactly a soft robotics hand; it is a soft robotics glove to help in the rehabilitation of people with chronic diseases (Figure 2.12(a)) [28]. It is formed by soft hydraulic actuators located on the dorsal side of the hand, that are constituted by moulded elastomeric chambers (Elastosil M4601) with fibre reinforcements. The article designates actuators as multi-segmented because they have different sections along the length. There are sections with the addition of a strain-limiting layer to provide bending, and in the thumb actuator, there are sections with different configurations of fibre reinforcement to provide bending and twist motion. The hardware system was designed in a portable and autonomous waist belt pack, with a closed-loop controller. A further case is a prosthetic hand composed of five pneumatically actuated soft fingers with stretchable optical waveguides for deformation sensing (Figure 2.12(b)) [29]. This waveguide has a transparent material allowing radiation losses to the outside that vary according to the deformation. With the aid of a photodetector, it is possible to measure the loss of power of the light and convert it into the corresponding deformation. Each finger consists of three waveguides and nylon fabric with slits on top of the fingers. Using the soft lithography method (explained in the following section), the waveguides were created with two different materials (VytaFlex 20, Smooth-On Inc. and

ELASTOSIL M 4601 A/B, Wacker Chemie AG), and the body of the fingers with silicone (Ecoflex™ 00 - 30). The palm of the hand was created by a 3D printer with a rigid material.

Deimel and Brock proposed the RBO Hand 2 (Figure 2.12(c)) [6]. It is a passively compliant and underactuated robotic hand that provides simpler controls, easy manufacturing and dexterous grasping. It is composed of seven pneumatic continuum actuators, called Pneuflex, five of them correspond to the fingers and the remaining two to the palm.

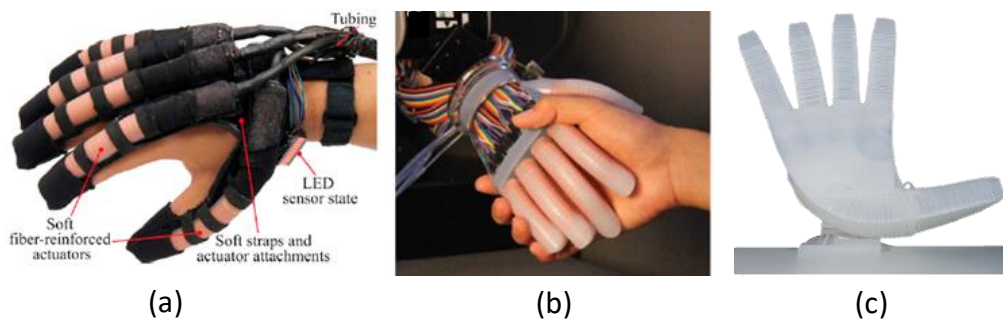


Figure 2.12. Three different concepts of soft robotics hands. (a) Soft robotics glove [28]; (b) Soft prosthetic hand via stretchable optical waveguides [29]; (c) The RBO Hand 2 [6].

Finally, Fras and Althoefer presented the soft pneumatic prosthetic hand [3],[30], with an appearance more similar to the real hand of a child (Figure 2.13(b),(c)). This hand has six actuators (fibre-reinforced conical actuator) and an exoskeleton structure that constrains the deformations of the actuators in the desired areas to led the actuator to move to the free areas (fingers joints) providing the bending motion. Each finger has one actuator and the thumb has two, to achieve the opposition and reposition motion. The manufacturing is made by pouring silicone material into the 3D printed moulds, providing a reduced cost. The actuators are built with soft silicone SmoothOn EcoFlex™ 00-50 and the exoskeleton with a stiffer silicone SmootOn SmoothSill 940. The actuators are driven by pneumatic pressure, from a control unit constituted by a Raspberry Pi computer and six solenoid valves, that are controlled independently with pulse width modulation (PWM) signals. This control unit can be executed by a joystick or using leapmotion controller, which consists of imitating the operator's hand. Some tests showed that the hand can perform several movements and it is capable to grasping various objects.

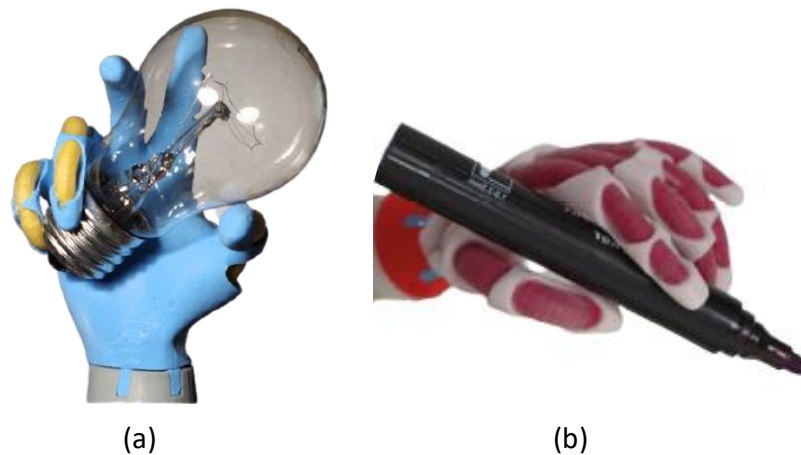


Figure 2.13. Soft pneumatic prosthetic hand. (a) Grasping a lamp [3]; (b) Grasping a pen [30].

2.4. Soft Robots Manufacturing

The rapid evolution of soft robotics is provided by the great development of design software and fabrication tools, where various processes are being studied. The most common manufacturing process consists of conventional moulding, with the use of elastomers which are poured and cured inside moulds produced by 3D printers. This process is often completed with another process, the soft lithography, where the components are constructed layer by layer (Figure 2.14) [9].

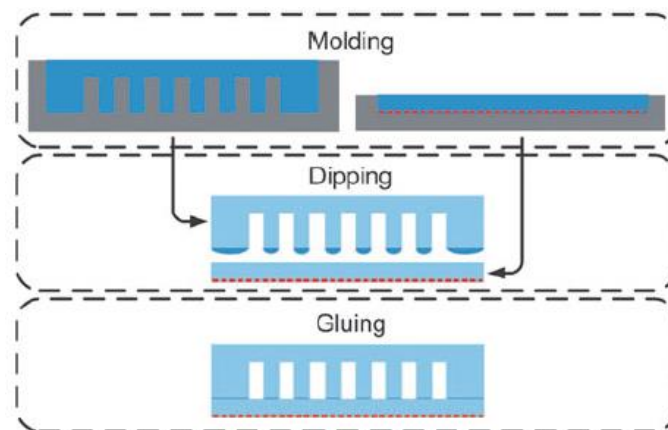


Figure 2.14. Soft lithography fabrication process for soft fluidic elastomer robots [9].

However, when the actuators are subjected to high pressures or even a significant number of pressurization cycles, this process may have limitations in the seams. In order to avoid the ruptures in these areas, the retractable pin casting process is used as an alternative [9]. Essentially, the structure is cast with a pin on the place of the channel, and after the structure is cured, the pin is removed, creating a channel with the shape of the pin.

Nevertheless, to be able to remove the pin, the channel structures of the actuators need to be relatively simple, also creating a limitation. Thus, to prevent the problem of seams and simple channels, the lost wax casting method has been proposed, where the space of the structure channels is filled with wax, and after the structure is cured, the wax can be melted and removed, creating the channels [31]. Even so, the structures produced are limited to those that allow the removable material to drain.

Looking at the processes described above, despite allowing the production of soft robots, they all require a lot of labour and time, reducing accuracy and repeatability. To make soft robotics level up, it is necessary to go further, as Walker et al. points out: “In order for soft robotics to gain foothold in industrial, military, and consumer spaces, production must move beyond existing methods. Soft robot fabrication technology must become automated and robots must be easily created at a relatively low cost and on large scale” [32]. Following this line of thought, the researchers began to focus on additive manufacturing (AM), also known as 3D printing. The most common types are fused deposition modelling (FDM) (Figure 2.15(a)), PolyJet (Figure 2.15(b)) and stereolithography (SLA) (Figure 2.15(c)). All of these three types can significantly reduce human manual work, saving time and increase the accuracy of components, but with the downside of not being able to manufacture with the same materials than conventional moulding processes.

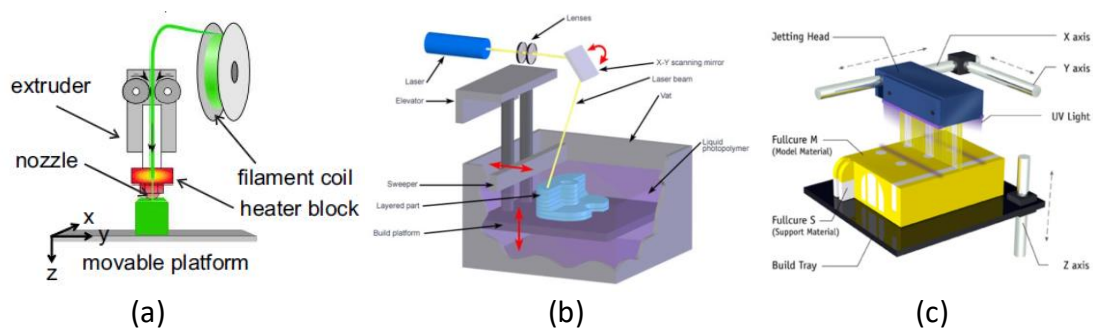


Figure 2.15. Three types of additive manufacturing (AM). (a) Fused deposition modelling (FDM); (b) PolyJet; (c) Stereolithography (SLA).

The first two methods, SLA and PolyJet, consist in photopolymerization technology, where the photopolymer materials are exposed layer by layer to radiation UV, creating high-resolution prints. However, according to [32], the photopolymers materials are limited by the low failure strain (at around 40% of strain), while others materials like polydimethylsiloxane (PDMS) used in conventional moulds can reach over 600% strain. At

last, 3D printing based on FDM, it is the most common and inexpensive method, creating good results in multiple conditions. Within this scope, the researchers in [33] developed a soft pneumatic actuator using the commercial Ninjaflex material. They have proven that this technique can be well applied in soft robotics applications such as manipulation, where it has shown great load-weight ratio and in wearable applications, where a customized glove was created to assist patients with hand motion disabilities. The only drawback of this process is the thermoplastic materials, such as Ninjaflex, which have significantly higher hardness values compared to PDMS or platinum cure silicones. To get an idea of the values, the Shore hardness of Ninjaflex thermoplastic material is eight times greater than PDMS [32].

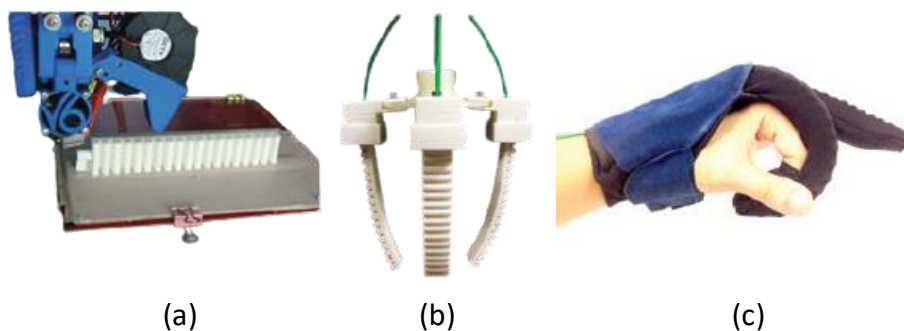


Figure 2.16. 3D printing with Ninjaflex material [33]. (a) Printed actuator; (b) A high force soft gripper; (c) Soft robotics hand exoskeleton to assist finger flexion.

With the purpose to combine the qualities of the 3D printing technology and the materials used in conventional moulding processes, some researchers have been exploiting a new alternative, that was designated to direct ink writing (DIW). This new process involves printing objects with a new extruder concept which has an active mixer and a temperature controller incorporated to allow the use of two-part platinum cure silicones [32].

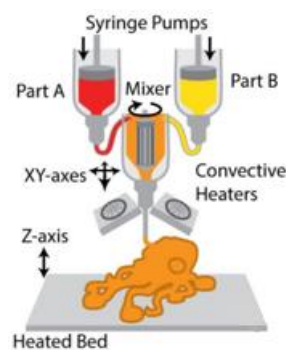


Figure 2.17. Direct ink writing scheme (DIW) [32].

From this extruder was conceived a four-channel tentacle (Figure 2.18 (a)), a quadrupedal robot (Figure 2.18(b)) and a pneu-net actuator (Figure 2.18 (c)), which were then subjected to experimental tests and compared with the same soft robots but manufactured with soft lithography and lost wax casting processes. This technique demonstrated that the 3D DIW could achieve or even improve the same results developed by the manual processes, supporting higher values of pressure, with less dimensional errors and with a significant reduction in manufacturing time. However, DIW printing requires the creation and application of an extruder on the printer, so currently, it is not yet a viable method.

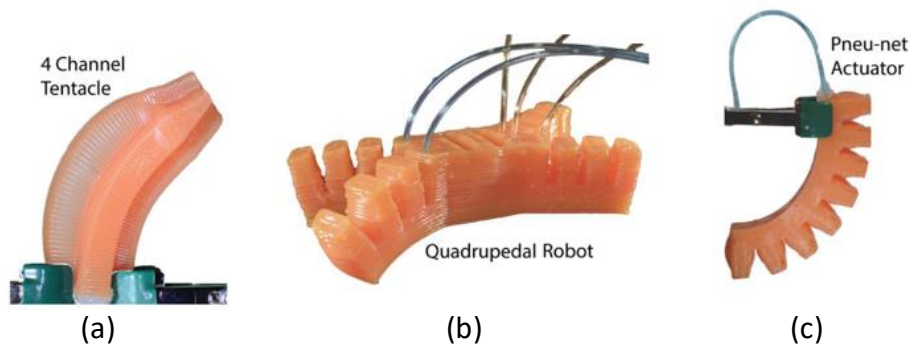


Figure 2.18. 3D printed soft robots based on DIW. (a) 4 channel tentacle; (b) Quadrupedal robot; (c) Pneu-net actuator.

2.5. Finite Element Analysis

In soft robotics, the actuators are inherent to the structure and they have an infinite number of DOF, so the control is more complex to predict and execute. Thus, the numerical simulation has been used to estimate and improve the possible configurations of one or several actuators. The Zhongkui Wang, et al., analysed different individual fingers designs based on pleated actuators and different grippers picking up the soft container, using the finite element method in the *Abaqus* software [20]. In [16], a general tool based on transient FEA was introduced, where the dynamic performance of soft surgical manipulators was designed and studied using *Ansys* software.

The Finite Element Method (FEM) is widely used in the numerical simulation of any physical phenomenon [34]. The use of FEM in real-time with the *SOFA* software was implemented and tested to obtain more accurate results. To this end, Lagrange multipliers were inserted to extract the reduced mechanical compliance in the areas of the actuators and

the end-effector position, and a constrained-based approach was solved by an iterative algorithm to find the contribution of the actuators in the deformation of the structure [35]. Still in *SOFA* software, an opensource for multi-materials simulations was recently launched, to facilitate the modelling of soft robots with different materials. It consists of a set of tools to help users to design partitioned tetrahedral meshes, with the aim of a single mesh to have different properties [36]. Gunjan Agarwal et al. [37] implemented a numerical method where the actuators under study are reinforced with an un-stretchable shell. Two different prototypes were studied (linear and bending actuators), consisting of a majority component with the elastomer Ecoflex™ 00-30 and an un-stretchable shell made of polyethylene terephthalate (PET). The numerical models were used to predict the actuator behaviour in large strains in order to execute design iterations for optimizations. Then the prototypes were subjected to experimental tests of free displacement and blocked forces, where the numerical models were validated.

In another context, the use of soft sensors is very important to obtain feedback regarding the control of soft robots. Nonetheless, obtaining feedback from these sensors is a tricky task due to the infinite number of DOF. For a better understanding, a soft capacitive sensor was placed inside of a soft pneumatic actuator, and with the aid of the development of a finite element model using the *COMSOL* software, it was studied how pressure, force and stretch influence the change in the capacitance of the sensor [38].

3. SOFT ROBOTICS HAND CONCEPT

3.1. Human Hand Anatomy

In order to obtain a robotic hand, which executes as many tasks as possible and ideally looks like a real hand, the study of some concepts of human hand anatomy is required.

The finger movements are produced by different muscles that are located in the hand and forearm. The forearm muscles narrow into tendons until they reach various points on the finger bones. Although the concepts related to muscles and nerves are quite important to understand the whole kinematics of the hand, in this dissertation, these contents will not be developed. The focus is only on the bones and their joints because these structures can reach the dexterity of the hand.

3.1.1. Bones and Joints

The human hand is composed of several bones with multiple joints (Figure 3.1) giving a vast number of movements with a high degree of stability, precision, strength and flexibility. This bone structure begins at the root of the hand, i.e. the wrist zone, which is composed of eight grouped bones, called carpals bones. The remaining posterior bones correspond to the composition of the fingers, containing metacarpals and phalangeal bones. Each finger presents one metacarpal bone and three phalanges, except the thumb that only presents one metacarpal bone and two phalanges bones. The metacarpal bone is the bone closer to the wrist, and the phalanges bones are divided into proximal, intermediate and distal phalange. The proximal phalange, according to the name, is the bone closer to the metacarpals, the intermediate bone is the middle and the distal bone is the last finger bone. In the case of the thumb, the intermediate bone does not exist.

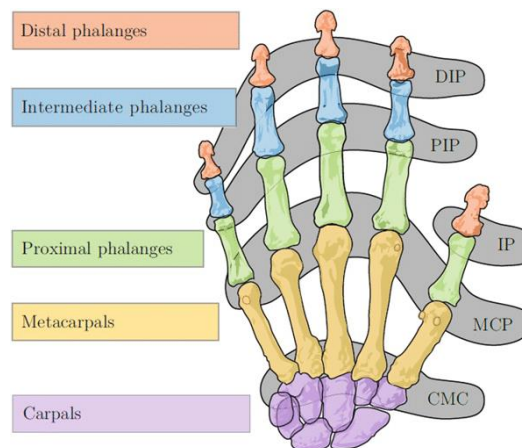


Figure 3.1. Bones and Joints of the Human Hand (left hand). CMC – Carpometacarpal, MCP – Metacarpophalangeal, IP – Interphalangeal, PIP – Proximal Interphalangeal, DIP – Distal Interphalangeal joints [39].

From the same Figure 3.1, the area of the joints can be seen in grey. The Metacarpophalangeal joint (MCP) is the joint between the metacarpal bone and the proximal phalange bone and, it enables to perform two distinct movements: flexion/extension and adduction/abduction, in other words, it has two DOF. In the connection of the three phalangeal bones, there are two Interphalangeal (IP) joints, except the thumb once again, with only one joint. These joints just have one DOF, making the flexion/extension movement with more capacity for flexion than for extension. The IP joints are distinguished by Proximal Interphalangeal (PIP) joint and Distal Interphalangeal (DIP) joint, to the same reason of the bone’s designations.

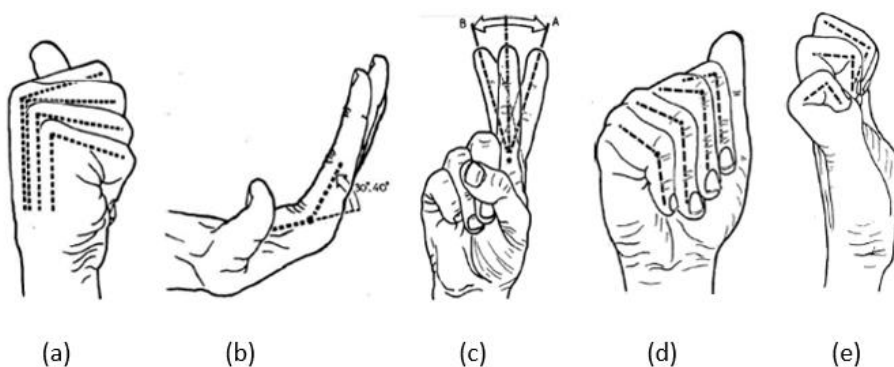


Figure 3.2. The motion of each joint; (a), (b) and (c) – Flexion, extension and abduction/adduction of the MCP joint, respectively; (d) and (e) – Flexion of the PIP and DIP joint, respectively [39].

A significant part of the human hand's capacities, mainly in the interaction and manipulation of objects, is due to the thumb. It differs from the others because it does not have the second phalange and also because it has high mobility in the Carpometacarpal

(CMC) joint. Unlike the CMC joint of the other fingers that have one DOF, the CMC joint of the thumb contains two DOF allowing flexion/extension and abduction/adduction. The MCP joint allows just like the other fingers to have two DOF, but with the advantage of the thumb to have a greater range of adduction/abduction angle. The IP joint just has one DOF. In this way, the thumb allows several movements as represented in Figure 3.3[39][40].

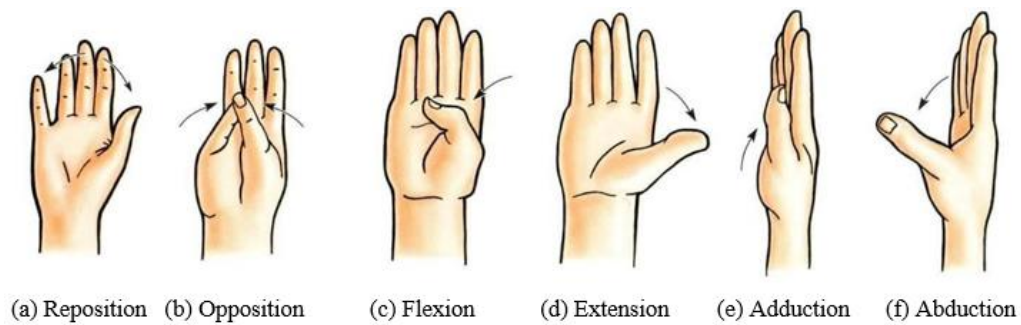


Figure 3.3. Thumb Movement Types [41].

3.1.2. Actuation Strategies

A recent study reports how the actuation strategy for underactuated hands affects the ability of a hand to grasp different objects and mimic the movements of fingers (anthropomorphism) [39]. In a first phase, the various grasps used by the human hand were studied, describing the existence of 33 different grasps [42]. Also, the most frequently used positions in daily life were studied. Then, 16 possible actuation configurations were defined, from 1 to 5 actuators and the positions of grasping objects that each strategy could achieve were analysed. The study consisted in determining which configuration achieves the most grasps, but also determining which configuration achieves the highest percentage of top10 grasps. In a second phase, a study about which configuration achieves the highest anthropomorphism index was carried out.

In a first conclusion, a larger number of actuators leads to better performance, however, the higher number, the more difficult it is in terms of space, control complexity, hand weight and cost. In a second conclusion, it has been described that it is advantageous to actuate the middle, ring and little finger simultaneously, and act the thumb and index finger independently. Also, the option of using an independent actuator for thumb abduction/adduction movement proved to be quite important for the actuation strategies.

3.2. System Requirements

According to the bibliographic review, there is potential to create a robotic hand with only soft materials, without metallic components, resembling the shape of a real hand, improving patient safety and improving compliance with different objects. Thus, in this dissertation, a robotic hand will be presented, where the main requirement will be the use of soft materials.

The development of the soft robotics hand consists of two main components: the structure and the fibre-reinforced actuators. The exoskeleton defines the hand structure, and the fibre-reinforced actuators will be inside of the finger's structure. The hand structure will be made of a stiffer material compared to the actuator, but it still would be a flexible/soft material. The fibre-reinforced actuators will be composed of an elastomer, which is a stretchable material with excellent flexion properties and high deformation capabilities, and another component will correspond to a polyethylene terephthalate (PET) helical thread, also known as polyester. This thread will be inserted in the middle of two layers of elastomer, operating as a reinforcement (Figure 3.4(a)). When the actuator is pressurized, the reinforcement prevents radial deformation, allowing only longitudinal deformation. The structure offers a configuration that allows constraining the deformation of the actuator in the area of the human hand bones, except in the area of the finger joints (Figure 3.4(b)). As the structure will also be closed at the fingertip, the longitudinal deformation of the fingertip will be constrained, and the actuators tend to expand to the free areas (finger joints), converting the longitudinal motion into a bending motion. This concept is based on the work of Jan Fras and Kaspar Althoefer [3][30], which has proved to be successful in grasping capabilities and manipulation tasks. However, here the manufacture of the hand structure is implemented by 3D printing.

The hand will have seven actuators, and they could be controlled independently, but also, they could be controlled in groups (synergistically) to reduce the control requirements. Each finger will be composed of one actuator, and the thumb will be composed of three, one for the flexion motion and two for the opposition/reposition motion. When the two thumb actuators are actuated, the opposition motion will be created, and when they are not actuated, the reposition motion occurs. They will be placed in the palm, close to the thumb, restricted on the tips and the palm side. As the palm side restriction will have a thin

thickness, and only the upper part will be freedom, when pressurized, the actuator tends to expand to the upper part, creating a bending motion (Figure 3.4 (c)).

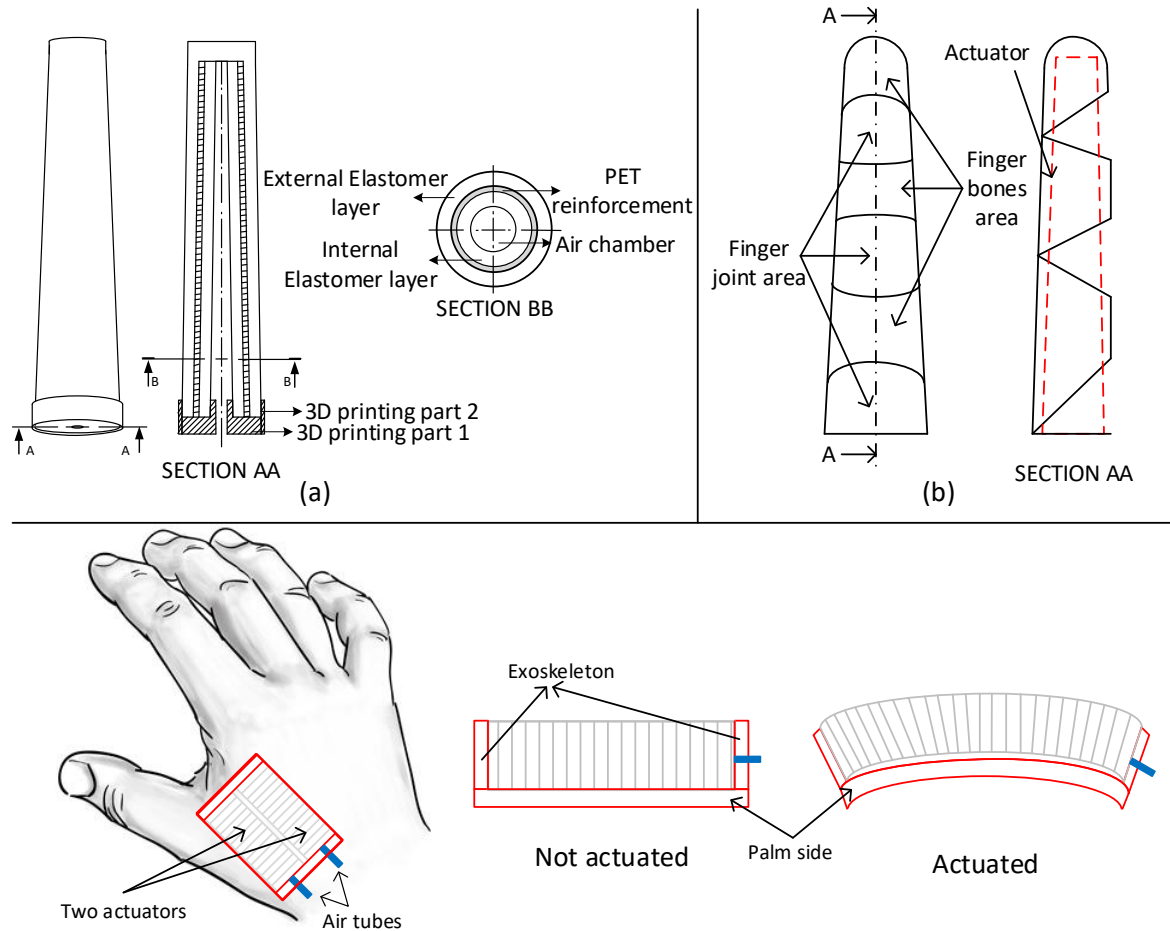


Figure 3.4. Concept of the soft hand fingers. (a) Fibre-reinforced actuator; (b) Finger exoskeleton; (c) Opposition/reposition thumb actuators.

3.3. Manufacturing

The manufacturing processes used will be the FDM and the pin casting, for the exoskeleton and the actuators, respectively. Both processes require a 3D printer, but with different purposes. For the first process, it will be used to 3D print directly the exoskeleton of the hand with flexible materials. In the second process, it will be used for the creation of the moulds that serve as auxiliary tools for the creation of the actuators.

The design of the hand and the actuators moulds are conceived using CAD software, more specifically, the *Autodesk Inventor 2020*. With the variety of tools that the program offers, it is possible to approximate the proposed hand to a real hand. The complexity of the hand would create difficulty in changing measures to create suitable

actuators and to make comparisons of results. Also, the high number of details of a real hand, in FEA, creates a high number of meshes that consequently would take many hours to run a simulation and therefore increases the likelihood of errors. For these reasons, the 3D scanning will not be used. The CAD file is saved in stereolithographic (STL) format, which is a file that only describes the geometrical surface of a 3D object, and this file is essential because the slicer software (next step) requires this type of format. After obtaining the STL file, it is loaded into the slicer software called *Ultimaker Cura*. This software slices the model into horizontal layers with the trajectories that the 3D printer needs to perform in order to build the object. After the successful slicing, the data is then saved in g-code format and transferred to the 3D printer, in this specific case, *BQ Hephestos 2*.

3.3.1. Materials

3.3.1.1. Elastomers

Elastomers are polymeric materials that when submitted to mechanical stresses, can highly deform and when the stress is removed, can return to the initial format (or almost). There are many types of elastomer materials such as natural rubber, synthetic polyisoprene, styrene-butadiene rubber, nitrile rubbers, polychloroprene and silicones. Among all types of elastomers, the only one referenced in this document is the silicones, once they will be the only ones used in the manufacture of the actuators. Silicone rubbers can operate in a wide temperature range (-100 °C to 250 °C), conceiving great advantage to this type of elastomers.

As silicon and carbon atoms have valence 4, they can form polymer chains through covalent bonds. Moreover, when silicon forms polymeric chains, and simultaneously there are silicon-oxygen repeating units occupying the main chain, the formation of silicones occurs. Between the most varied types of silicones elastomers, the most common is that in which groups of methyl are attached to silicon, calling themselves polydimethylsiloxane (PDMs) [42].

Recently, other types of silicones are used in soft robots. They are platinum-catalysed silicones, highlighting the Ecoflex™ rubber and the Dragon Skin™ 30, both produced by SmoothOn, Inc. According to the manufacturer, these silicones are suitable for making moulds for casting but also for making prosthetic and orthotic devices [43]. The

disadvantage of using these materials is that they are patented and exclusive to the manufacturer, making it difficult to search for information on their composition and chemical structure which helps to obtain the optimum conditions for manufacturing processes. However, there are several examples in bibliographic review that allow concluding the potential of these materials in the application of soft robots.

Table 3.1 shows the properties of three platinum-catalysed silicones, often used in applications of soft robots. In general, if the goal is to choose a silicone with good elongation capacity, the choice of Ecoflex™ 00-50 will be the most pertinent. However, if the choice is the most resistant material, then Dragon Skin will be better due to the higher tensile strength. According to Smooth-On, the hardness can be classified in three levels (Figure 3.5), Shore hardness 00, Shore hardness A and Shore hardness D, which range from measurements of very soft rubbers and gels to measurements of hardness of hard rubbers, semi-rigid plastics and hard plastics [44].

Table 3.1. Technical overview of three platinum-catalysed silicone types.

Silicone types	Cure time [hours]	Pot life [min]	Density [g/cc]	Shore hardness	Elongation [%]	Tensile strength [MPa]	Tensile Modulus [MPa]
Dragon Skin™ 30	16	45	1.08	30A	364	3.447	0.593
Ecoflex™ 00-30	4	45	1.07	30A	900	1.37	0.0689
Ecoflex™ 00-50	3	18	1.07	50A	980	2.17	0.0827

Since elongation is a crucial parameter for the finger movement requirements, the choice should be decided between the two Ecoflex™. Comparing them, Ecoflex™ 00-50 presents higher elongation, higher tensile strength and higher hardness. Also, the Ecoflex™ 00-50 has a shorter cure time. So, the choice falls on the Ecoflex™ 00-50 because it provides greater elongation and simultaneously greater tensile strength and hardness to withstand higher pressures.

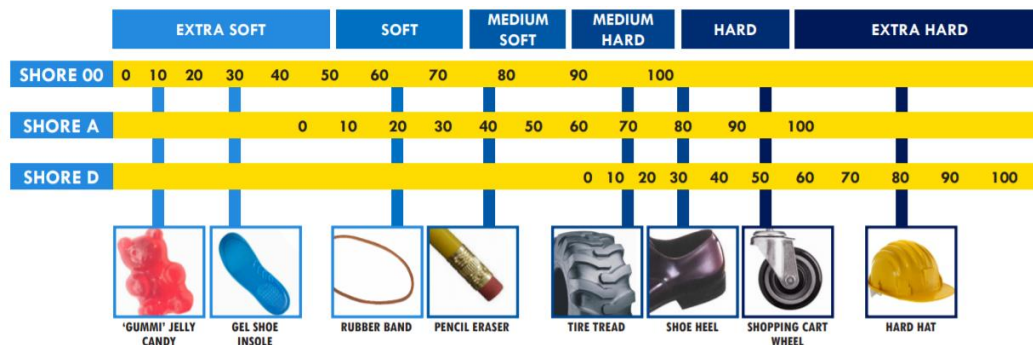


Figure 3.5. Shore hardness scales of SmoothOn, Inc.

3.3.1.2. 3D Printing Materials

Actually, common 3D printers are able to print a wide variety of thermoplastics. The most common materials are PLA and the acrylonitrile butadiene styrene (ABS). However, there are many more with similar characteristics: low flexibilities and relatively high hardness. Beyond these materials, in the last years have been developed flexible materials for 3D printer with lower hardness. These materials are thermoplastics elastomers (TPE) which result from a combination of thermoplastics and elastomers. The TPE are subdivided into six classes according to chemical structure, but only three are used for 3D printers [45]:

- Thermoplastic polyurethane (TPU);
- Thermoplastic co-polyester (TPC);
- Thermoplastic polyamide (TPA).

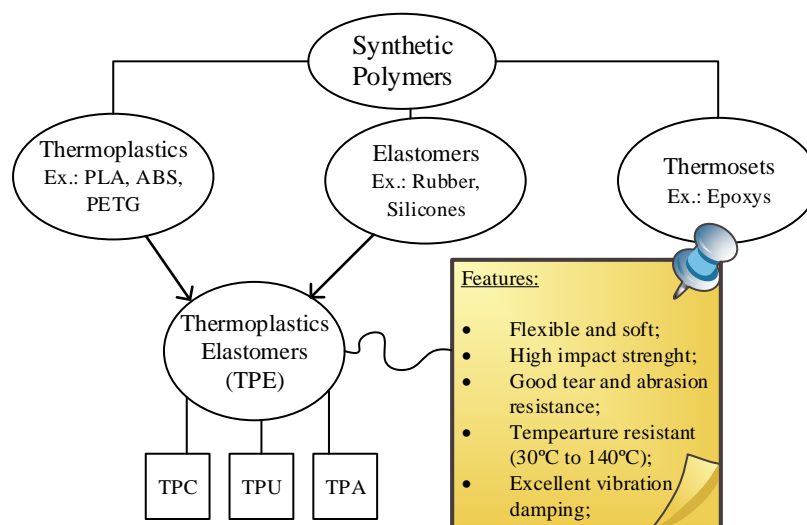


Figure 3.6. TPE formation diagram.

For the exoskeleton to be able to conceive bending motions, it will be necessary to present a higher stiffness compared to the actuator, to restrict the deformations of the actuator in the desired places. Therefore, the choice of TPE is a good option because it has higher stiffness than elastomers and at the same time, it has excellent flexibility capabilities. In Table 3.2, three of the most commercialized TPE are mentioned with the most relevant mechanical properties. There are many other models, but all of them with similar characteristics. Of the three materials, Filaflex 95A has the highest hardness value. The hardness value is directly related to the stiffness, and there is a need for the stiffness value of the exoskeleton to be higher than the actuator. However, if the hardness value is very high, consequently the stiffness value of the skeleton will also be, causing a decrease in the bending capacity of the exoskeleton. Therefore, Filaflex 95A material may not be a good choice and, of the three materials, it has the lowest elongation value. Between the two remaining materials, the hardness and elongation values are similar. As for the tensile strength, the value of Ninjaflex is lower; however, it is a value that, according to the solicitation of the actuator will be very far from being reached. Finally, the material chosen was Ninjaflex, not exactly because it has an advantage over Filaflex, but because the research community provided good comments about the printing of this material. However, with pre-existing Filaflex 82A material in the laboratory, a finger exoskeleton was printed (Section 4.1) and also proved to be an excellent option.

Table 3.2 Technical overview of three TPE materials.

Silicone types	Density [g/cc]	Shore hardness	Elongation [%]	Tensile strength [MPa]
Ninjaflex	1.19	85A	660	26
Filaflex 82A	1.12	82A	650	45
Filaflex 95A	1.00	96A	500	55

4. DESIGN AND IMPLEMENTATION

4.1. Finger

In a first phase, the design process focused on a single finger, respecting an iterative methodology towards continuous improvements to reach the requirements. The requirements are: (1) design with two different components (exoskeleton and fibre-reinforced actuator), (2) bendability, (3) use pre-existing laboratory materials (Filaflex 82A and SmoothOn Ecoflex™ 00-30).

4.1.1. Dimensions

The finger structure was designed with an external length of approximately 86 mm and an internal length (actuator length) of 76.5 mm. The radial thickness has been designed with 1.5 mm to offer the maximum possible flexibility. The internal diameter varies according to the length, with the largest value of 18mm at the base and the smallest value of 13.5mm at the tip.

4.1.2. Manufacturing

4.1.2.1. Finger structure

The finger was designed in CAD and manufactured on the 3D printer, following the steps described in Section 3.3. It was printed with Filaflex 82A material (Figure 4.1), whose printing parameters are available in Appendix B.

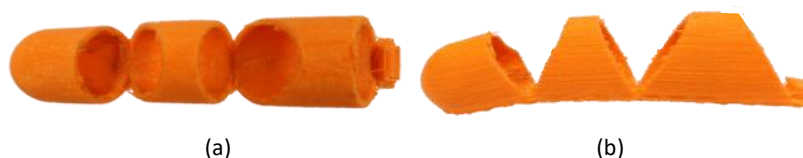


Figure 4.1. Finger exoskeleton made with Filaflex 82A material. (a) Top view; (b) Front view.

4.1.2.2. Fibre-Reinforced Actuator

The fibre-reinforced actuator contains two layers of silicone Ecoflex™ 00-30 separated with a reinforcement of PET helical thread with 0.25 mm of diameter. To create

this concept it was necessary to develop: a mould (Figure 4.2.(a),(b),(c)), two conical cores (Figure 4.2.(d)(e)), the preparation of the silicone mixture and a PET helical thread.

The moulds and conical cores were properly designed in CAD and printed on the 3D printer with PLA material. Moreover, the mould and the cores were coated with XTC-3D™ to ensure a better removal of the casting material.

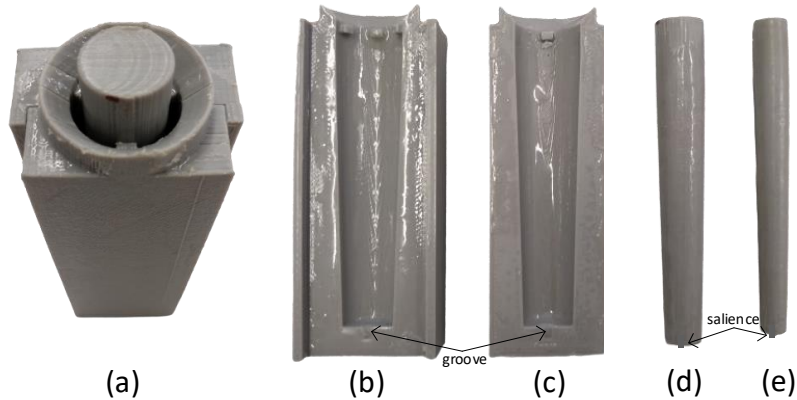


Figure 4.2. PLA printed parts. (a) Mould assembly with the largest core; (b) and (c) Mould parts; (d) Largest core; (e) Smaller core.

The thread is wound around the largest core, which is then placed inside the mould, and filled with the silicone. In this step, it was necessary to ensure that the thread was not too tight to the core, making it easier to remove after cure. When the material is cured, and the core is removed, as the PET does not adhere to the PLA but adheres to the silicone, the reinforcement remains together with the silicone creating the outer layer of the actuator. Next, for the manufacture of the inner layer, the other core is placed inside the already created actuator layer, and then it is again filled with silicone.



Figure 4.3. Fibre-reinforced actuator.

As is observed in the mould (Figure 4.2(b), (c)), there is a small groove in order to fit the salience of the tip of the cores to ensure centring. However, this step creates a hole in the tip. So, after creating the inner layer, silicone was added at the tip from the inside of the actuator to fill the empty space and create an extra thickness (2 mm).

For the base of the actuator (extremity corresponding to the air pressure inlet), a PLA part was created with a hole for the pipe connection. This part with the aid of a cable tie allowed to prevent the air leakage (Figure 4.4). The clamp process is not the most suitable, but as already mentioned, the purpose of the finger creation was only to test the general requirements.

4.1.3. Testing and Results

In general, a good motion of the finger folding was observed, with a good performance of the actuator that confirmed the potential of the PET reinforcement. Also, it was verified that after the pressurization, the finger could return to the un-actuated state. However, with some attempts, some leaks began to appear at the actuator tip, which was rectified, but after some attempts, the reliability was reduced again. The reason for these leaks comes from the manufacturing step that corresponds to centralize the core with the mould.



Figure 4.4. Assembly of the finger exoskeleton and the fibre-reinforced actuator.

4.2. Hand

According to the finger results, it was possible to conclude that the process, in general, has the potential to be used in the hand manufacture. In this way, the exoskeleton was again produced by 3D printing and the actuator by the same manual method, being applied some modifications that will be described subsequently.

4.2.1. Hand Design

The hand contains seven independent fibre-reinforced actuators, one actuator for each finger and two actuators for opposition and reposition motion of the thumb. The size of the hand was based on the dimensions of an adult hand, with 195 mm from the wrist to the tip of the middle finger. The radial thickness of the finger exoskeleton has 2 mm. Compared

to the finger created in the previous section, it was increased 0.5 mm to ensure that there would be no material breakage in the most requested regions. The main remaining dimensions of the exoskeleton and the fibre-reinforced actuators are presented in Appendix B.

4.2.2. Manufacturing

4.2.2.1. Exoskeleton

The hand exoskeleton was printed with Ninjaflex material (Figure 4.5), according to the choice described in Section 3.3.1.2. The printing parameters are available in Appendix B. As the geometry of the CAD hand does not have any flat side, to print the hand, it was necessary to activate the option to insert support material. Thus, at the end of printing, it was necessary to remove this excess material.

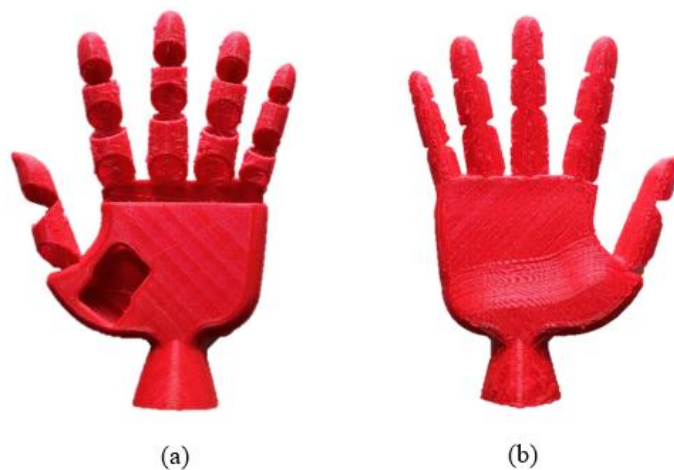


Figure 4.5. Hand exoskeleton. (a) Back side; (b) Palm side.

4.2.2.2. Fibre-Reinforced Actuators

Five actuators with different sizes were constructed with the same manufacturing procedure of the actuator mentioned in the previous section. However, there were three significant changes:

- Changing of silicone rubber material;
- Changing of the diameter reinforcement material;
- New mould design.

The silicone rubber material of the actuator was changed from Ecoflex™ 00-30 to Ecoflex™ 00-50, according to the choice obtained in Section 3.3.1.1. The material of the fibre-reinforced actuator was changed from another PET, but with 0,15 mm of diameter.



Figure 4.6. Polyethylene terephthalate thread.

As for the new mould design, the main reason for changing the moulds was to avoid the problem mentioned in the previous finger. The creation of a hole in the tip of the actuator due to the existence of a salience in the core to centre the mould. This problem required the addition of silicone in a next step to seal the tip, but as the tip is the most solicited zone of the actuator, a new solution had to be found to avoid issues and assign more reliability to the actuator. In this way, the new designed concept allows the cores to be suspended and centred in the mould with the necessary space between the core tip and the mould to cure the silicone layers, without any additional step (Figure 4.7).

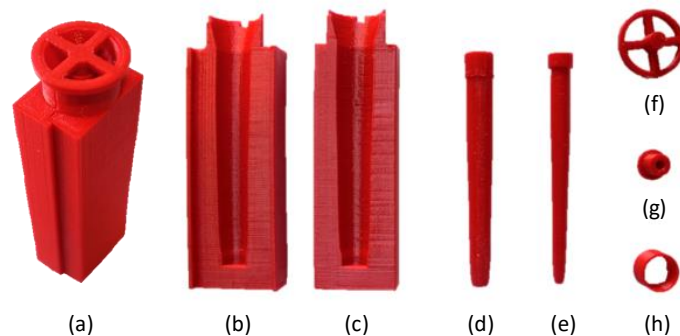


Figure 4.7. 3D printing parts for the construction of the actuators. (a) to (f) mould parts; (g) and (h) actuator parts.

To build a fibre-reinforced actuator, four main steps were performed: fabrication of the 3D moulds (I), outer layer with the reinforcement (II), inner layer (III) and seal the base (IV). As each finger has a different geometry, five different moulds have been created. For the step (II) and (III), a main mould (Figure 4.7 (a),(b),(c)) with two cores with different sizes (Figure 4.7 (d),(e)) and the part represented in the (Figure 4.7 (f)) were required. With this last part, it was possible to suspend the cores in the centre of the mould,

because the cores are connected to this part which in turn are connected to the main mould. For the last step (IV), two parts were created (Figure 4.7 (g) (h)) to seal the actuator.

Turning to the detail of all manufacturing steps, it was necessary to start with the explanation of the silicone rubber Ecoflex™ 00-50 preparation. This material is available in two containers with different chemical constituents, whereby, before casting into the mould it was followed the brand instructions that are presented below.



Figure 4.8. Silicone rubber Ecoflex™ 00-50.

1. The containers (Part A and B) were completely stirred before dispensing.
2. The required amounts were spilt into two containers (one for each part) in order to display the 1:1 ratio of material volume. Another alternative would be by material weight.
3. The two silicone components were put together and mixed for at least 3 minutes, ensuring that the edges of the container have been scraped several times. This step required great caution to avoid as much as possible the trapped air due to the lack of an optional step that corresponded to vacuum degassing for 2-3 minutes.
4. When the mixture looked to have little trapped air and a low viscosity, then it was ready to be poured. From experience, letting the mixture settle for some time reduces the number of trapped air. In order to avoid the cure of the mixture, it was estimated to wait about 1 minute to settle.

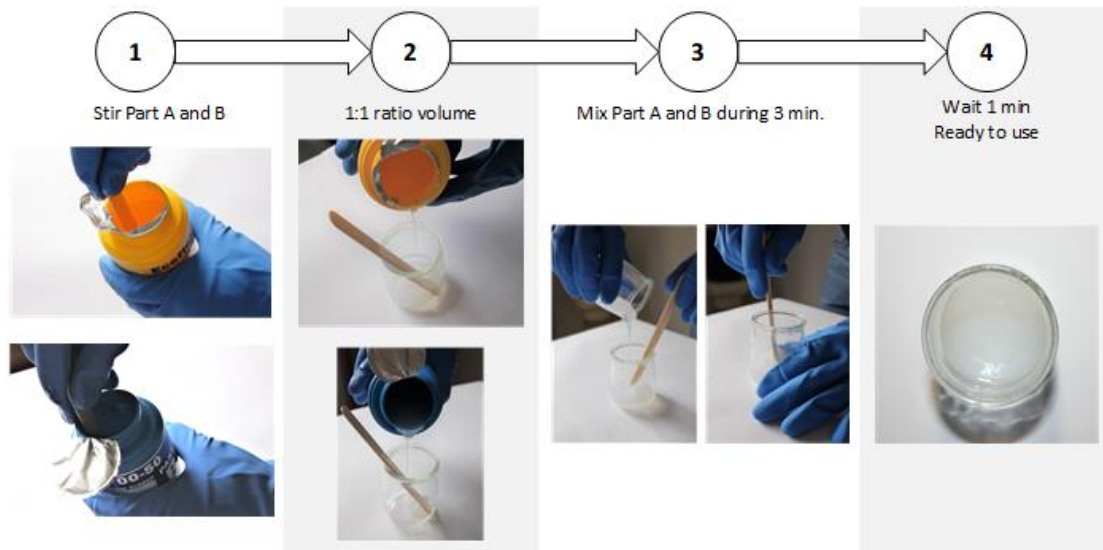


Figure 4.9. Preparation of Ecoflex™ 00-50 before casting.

Between each main step of the actuator construction (II and III), it was necessary to wait the curing time of the silicone, so the preparation described was repeated two times. To achieve the maximum results of the material, the brand advises to cure the material at room temperature (23 °C) or at least to not cure it under 18 °C. The cure time of Ecoflex™ 00-50 is three hours and it is also recommended after the cure time at room temperature to expose the silicone to 80°C for 2 hours and 100 °C for one hour, and after that to let it cool down to room temperature again. These recommendations are adequate to quickly reach maximum physical and performance properties.

After the silicone is ready to casting, the container is tilted slowly so that the material pours smoothly in order to prevent the formation of new air bubbles. The material is gradually poured so that it has time to settle down and release the trapped air.

Now explaining the procedures, the step (II) started to wrapped the PET thread to the largest core, and after, the silicone was poured into the mould. It is important that the thread is completely clean and whenever possible attached without the aid of any adhesive tape, since that is enough for the layer to be poorly sealed. When the first layer was cured, the mould was opened and the core was removed from inside of the layer. As the PET does not adhere to the PLA but adheres to the silicone, the reinforcement remains together with the silicone. Still, this step is the most complicated and requires great care to pull the silicone in order to not disintegrate the reinforcement.

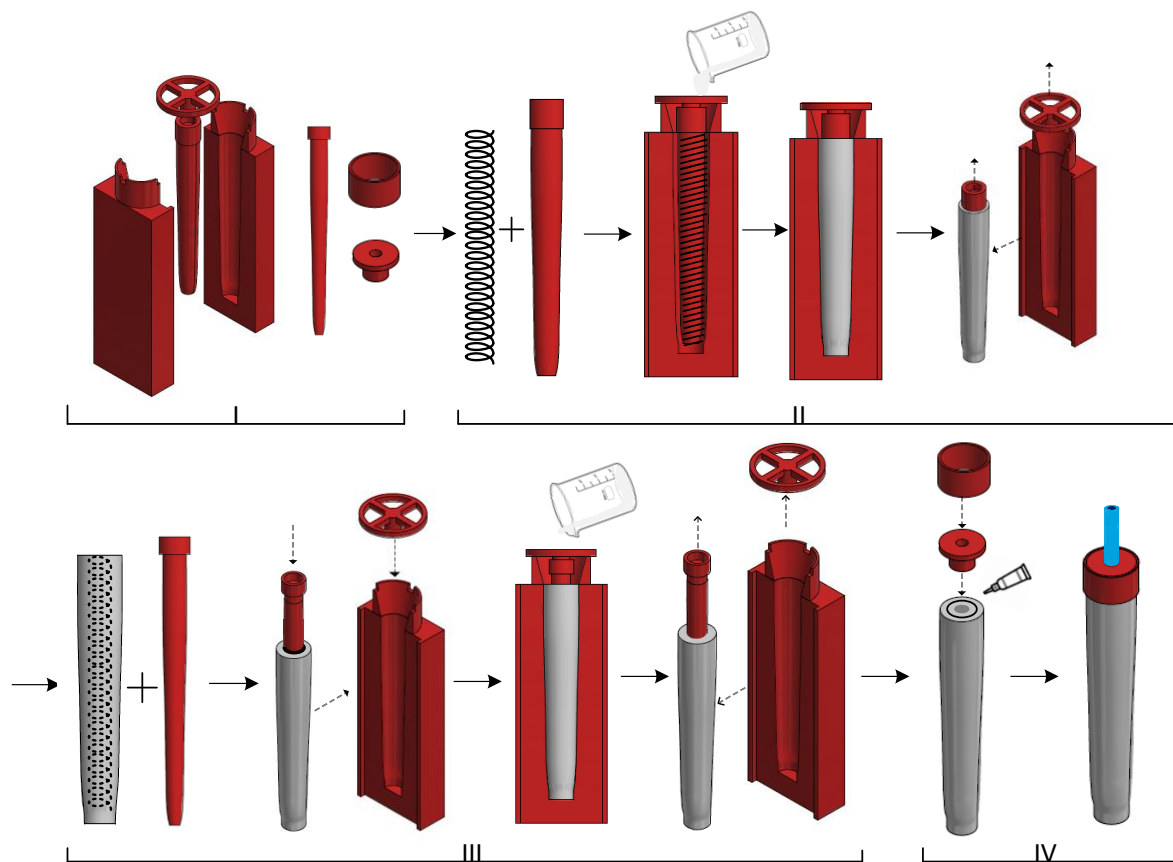


Figure 4.10. Mould concept used in the construction of the actuators.

Next, to create the second layer of the actuator (III), the first one already cured is put back into the mould but this time without the largest core. As the second core has smaller dimensions, there is a gap between the internal reinforcement and the core that defines the thickness to be deposited of material for the creation of this second layer. Thus, after preparation of the silicone again, it was deposited and cured. The removal of this layer is relatively easier due to the fact that there is no coiled thread, but still has to be removed with a considerable amount of care.

Finally, the last step (IV) consisted to seal the actuator base and creating a hole to insert the air inlet tube. With some failed attempts at this step due to air leaks around the pipe, a part was invented (Figure 4.7(g)) and inserted into the internal channel in the base of the actuator. In this way the tube fits precisely and eliminates the gaps that silicone allowed for air leaks around it. To ensure that the actuator is well sealed and also to provide a good fit on the exoskeleton, another part has been created (Figure 4.7(h)) and placed around

the previous part. Both parts were glued with super glue Loctite 401 that exhibit a high curing speed.



Figure 4.11. Fibre-reinforced index actuator.

4.2.3. Testing and Results

The results presented in this section only focus on hand manufacturing since the pneumatic control system has not yet developed. However, in the following chapter, the index finger has been pressurized manually with the aid of a pressure sensor (MPX4250AP) programmed in Arduino, where it is possible to observe the motions of the index finger when subjected to different pressure values.

Concerning the manufacture of the exoskeleton, 3D printing proved to be an excellent option, presenting high quality and dimensional precision, where the finger area exhibited the necessary flexibility to perform the folding. In the palm area, during the 3D printing, it was necessary to create support material, therefore, some surface imperfections were present when the support was removed. In addition, the thumb area on the palm became more rigid than expected, and it was not possible for the two actuators mentioned in section 3.2 to perform the opposition/reposition movement. However, the latter problem described was due to an exaggerated allocation of thickness in the CAD design and not because of the printing. The hand 3D printing required about 30 hours to be concluded.

The actuators created have proven that their overall concept works well and that they have the capabilities to actuate the exoskeleton. They can resist the necessary pressures, where the concept of PET reinforcement has been validated, avoiding radial deformations and favouring longitudinal deformations. However, the construction process has shown great manual care, requiring some attempts to create actuators of acceptable quality. The reason for this is due to the porosities (air bubbles) that occur during deposition and cure.

In the assembly (Figure 4.12), when the actuators were pressurized manually, it was found that the concept described in section 3.2 works perfectly, where the motions of

the fingers showed good bending motion, proving that 3D printing with flexible materials has great potential.

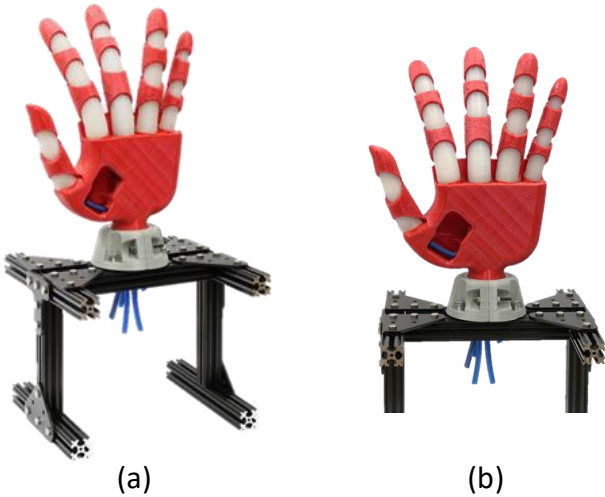


Figure 4.12. Soft pneumatic hand. (a) Isometric view; (b) Front view.

5. NUMERICAL MODELLING OF THE FINGER FOLD

5.1. Non-linear Analysis and Hyperelastic Materials

Most engineering applications use metallic materials, where the stress-strain curve that characterises the material have two distinct areas (Figure 5.1). The left-side area which corresponds to the elastic regime (linear), where the material properties are linear, and the Hooke's law defines perfectly the mechanical behaviour, and the right-side area which corresponds to the permanent and non-linear deformations.

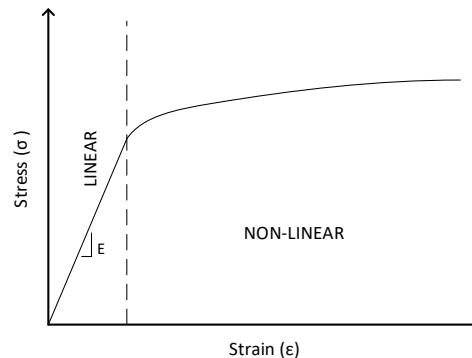


Figure 5.1. A typical stress-strain curve of a metallic material. Linear and Non-linear areas.

Typically, the design of mechanical systems is carried out assuming the mechanical components (from metallic materials) are working in elastic regime. Therefore, most of the numerical analysis are performed assuming a linear elastic behaviour of the mechanical components. Thus, the analysis is simplified because the materials under consideration are always contained in the elastic regime, where Hooke's law is applied with great precision due to the model's constant stiffness. The modulus of elasticity (E), the coefficient of Poisson (ν) and ultimate tensile strength (σ_s) are enough to describe the analysis.

However, not all numerical analyses can be considered linear, because in some models there are stiffness changes. Mostly, these changes arise from three factors: the geometry of the model (large deformations), the non-linear material, or the boundary conditions (loads and constraints, contact interaction)[46][47]. In the next sub-chapter, the choice of non-linear analysis was necessary because the three factors occur simultaneously.

The geometry of the finger presents large variations during the loading since the large displacements are required to describe the final geometry of the finger. The materials (TPE and elastomers) used present an hyperelastic behaviour defined by a non-linear response. Moreover, the frictional contact between the actuator and the exoskeleton are required, allowing sliding and separations of some regions of the bodies.

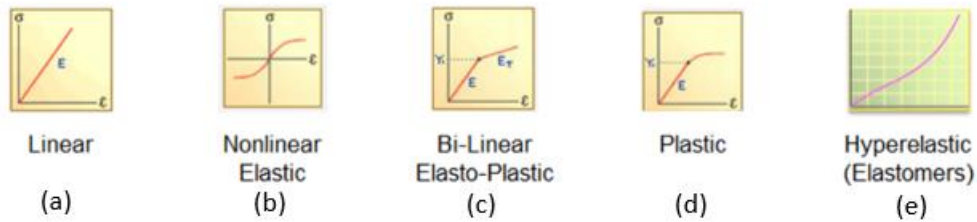


Figure 5.2. Different material behaviours. Visualization of the stress-strain curve for: Linear, Nonlinear Elastic, Bi-Linear Elasto-plastic, Plastic and Hyperelastic materials.

In the specific case of TPE and elastomers, they are considered as isotropic, non-linear elastic, and incompressible materials. As can be seen in Figure 5.2(e), these materials cannot be characterized as linear. To describe the mechanical behaviour, several hyperelastic materials models (Table 5.1) were developed to define the stress-strain relationship, using the strain-energy function (W) [48].

Table 5.1. Different models to characterize hyperelastic materials: Neo-Hookean, Ogden, Yeoh and Mooney-Rivlin[48],[33].

Hyperelastic model	Strain-energy function
Neo-Hookean	$W = c_i(I_1 - 3)$ c_i – material parameters I_1 – deviatoric strain invariants
Ogden	$W = \sum_{i=1}^N \frac{\mu_i}{\alpha_i} (\lambda_1^{\alpha_i} + \lambda_2^{\alpha_i} + \lambda_3^{\alpha_i} - 3)$ μ_1, α_2 – empirical parameters $\lambda_1, \lambda_2, \lambda_3$ - principal stretches
Yeoh	$W = \sum_{i=1}^3 c_i (I_1 - 3)^i$ c_i – material parameters I_1 – deviatoric strain invariants
Mooney-Rivlin	$W = \sum_{i=1}^2 c_i (I_i - 3)$ c_1, c_2 – material parameters I_1, I_2 – deviatoric strain invariants

In the study [49], uniaxial tensile tests were performed on three different silicones (Ecoflex™ 00-30, Ecoflex™ 00-50 e Dragon Skin™ 30). The tests were executed with 30mm-6mm-3mm samples on an Instron testing machine with a 100 N load cell at a speed of 300mm/min of the transverse head. Then, the hyperelastic models were adjusted to the experimental data in the strain range of 0-300%, where the use of least squares methods allowed to obtain the best model for each material and the respective coefficients of the deformation energy equations (Table 5.2).

Table 5.2. Parameter values of different hyperelastic models to characterize Ecoflex™ 00-30, Ecoflex™ 00-50 and Dragon Skin™ 30 materials [49].

Material	Hyperelastic model	Coefficients	Parameter value (MPa)
Ecoflex™ 00-30	Yeoh	N	3
		C_{10}	5072
		C_{20}	-331
		C_{30}	-15
Ecoflex™ 00-50	Ogden	N	3
		μ_1	107.9×10^3
		α_1	1.55
		μ_2	21.47
		α_2	7.86
		μ_3	-87.1×10^3
Dragon Skin™ 30	Yeoh	N	2
		C_{10}	1190
		C_{20}	23.028

Also, in the study [33], with the TPE Ninjaflex, uniaxial tensile tests were performed following the ISO 37 standard, in which the samples were stretched using Instron Universal Tester 3345. The material parameters involved in the models were adjusted to the experimental data obtained in the strain range of 0-500% with the *Abaqus* software, where the least square curve fit was once again applied to determine the coefficients for each model (Table 5.3). To understand which was the best model to characterize the material, the author determined the sum of square error for each one and concluded that the Ogden model was the most suitable for Ninjaflex.

Table 5.3. Parameter values of different hyperelastic models to characterize Ninjaflex material [33].

Hyperelastic model	Coefficients	Parameter value (MPa)	Sum of square error (sse)
Ogden	μ_1	-30.921	0.644
	α_1	0.508	
	μ_2	10.342	
	α_2	1.375	
	μ_3	26.791	
	α_3	-0.482	
Mooney-Rivlin	C_{10}	0.677	45.280
	C_{01}	1.621	
Yeoh	C_{10}	1.653	159.481
	C_{20}	0.0324	
	C_{30}	0.000486	

In both studies only uniaxial tests were performed, so the models are only adjusted to the stress-strain curves of these same tensile tests. However, it recommended performing other experimental tests, such as biaxial tests, simple and pure shear tests.

5.2. Development of the Computational Model

The numerical analysis of the system was carried out using software *Autodesk Inventor Nastran*®. The computational model was developed to simulate the capabilities of the fibre-reinforced actuator when working in conjunction with Ninjaflex exoskeleton. The creation of a model allows to predict several results and optimize geometries for better performance without spending resources and saving time.

The entire computational model detailed below only pertains to the index finger since it would be the same principle for the other fingers. The design of the hand exoskeleton consists of only one CAD file, but due to the high detail, the simulations was slower, and there was more chance to suffer convergence problems. Since the study only focuses on the index finger, to simplify, the hand exoskeleton CAD has been cut off, creating a solid of the index finger (Figure 5.3).

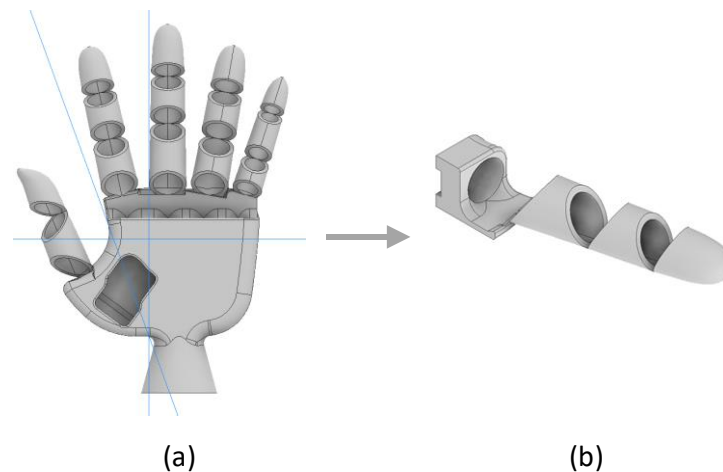


Figure 5.3. Simplification of the model. (a) Hand design with visualization of the plans to cut off the finger - CAD file; (b) Index finger exoskeleton - CAD file.

The main goal of the FEA was to predict the mechanical behaviour of the index finger, namely the maximum vertical displacement and the maximum finger folding angle. These two types of results have been designated as the most relevant because the primary function of a hand is to bend the fingers to achieve excellent manipulation and dexterity characteristics. Nevertheless, before running this numerical model, it was necessary to ensure the best numerical characterization of the materials. Therefore, two types of simulations combined with experimental tests were previously performed. The goal was to analyse the accuracy of the parameters obtained in the literature review, and if necessary, change them to bring them closer to reality. In addition, these simulations helped to predict the behaviour of the actuator and the exoskeleton individually, when subjected to different loads. The two types of simulation are divided into the hand exoskeleton (Ninjaflex) and the actuator (Ecoflex™ 00-50 with PET) which are described below in detail.

5.2.1. Exoskeleton

To verify the coherence of the materials model parameters previously obtained, numerical simulations and experimental tests were performed with different forces applied to the fingertip of the exoskeleton. The comparison between numerical simulations and experimental tests allowed to observe the difference in the characterization of the material and use the necessary adjustments. In both cases, the maximum vertical displacements for each force were annotated. The value of the forces corresponds to the finger's own weight and weights of 7 g, 16 g, 28 g, 41 g and 57 g suspended by a thread.

For the experimental tests, the palm of the exoskeleton was placed over a surface leaving only the fingers hanging. Then, a millimetre sheet of paper was placed between the index finger and the middle finger to obtain the displacements easily and accurately (images on the left side of Figure 5.6). The reference value used to measure the displacements were the bottom surface of the exoskeleton palm. The experimental measurements were repeated three times, and afterwards, the average was determined (Table 5.4).

Table 5.4. Measurements of the maximum vertical displacements of the index finger obtained experimentally when subjected to: own weight, 7 g, 16 g, 28 g, 41 g and 57 g.

Force (N)	Vertical displacement (mm)			
	EXP1	EXP2	EXP3	$\overline{\text{EXP}}$
0.00	46.0	46.0	44.0	45.3
0.07	66.0	64.5	63.0	64.5
0.16	74.0	75.0	74.5	74.5
0.27	79.0	80.5	80.0	79.8
0.40	80.0	83.0	83.0	82.0
0.56	82.0	86.0	85.5	84.5

For the non-linear FEM, the Mooney-Rivlin model was chosen to characterize the hyperelastic material Ninjaflex. According to the Hong Kai Yap et al. [33], the best model was the Ogden; however, when tried to apply in this model, the simulation did not converge. So, the decision to choose the Mooney-Rivlin model was based on being the second model with the lowest sum square error value (Table 5.3). The parameters used are in Table 5.5, designated as “MR set 1,2 and 3”. The parameters “MR set 1” are the values obtained by the study [33] and the next two sets of parameters are the adjustments implemented to achieve closer the experimental results. Another critical parameter in the characterization of the model materials is the incompressible value (D). This parameter defines the volume variation when subjected to a load. In the case of hyperelastic materials, there is a fully incompressible or nearly incompressible behaviour. Although fully incompressible behaviour is not available in *Autodesk Inventor Nastran*®, nearly incompressible can be implemented using a large value of D, therefore, a value of $D = 1 \times 10^5$ has been assigned. About the density of Ninjaflex, the value attributed by the producer is 1.19 g/cm^3 . This property is not very relevant when applying pressure since it makes the influence of gravity insignificant. However, for experimental tests with weights, it is an asset to achieve the experimental values. The density of the material producer may

be different from the real one because the 3D printing can change the original mechanical properties. So, the calculation of the new density after the 3D printing was made. The 3D printed exoskeleton was weighed, and the total volume was obtained from the CAD file,

$$\rho = \frac{m_{exoskeleton}}{V_{CAD}} = \frac{92\text{ g}}{111,209\text{ cm}^3} = 0.827\text{ g/cm}^3, \quad (5.1)$$

where ρ is the density, m is the weight and V is the volume. The real density is lower than that given by the producer.

Table 5.5. Set of parameters of the Ninjaflex Mooney-Rivlin model. MR set 1 – Taken from the article [33]. MR Set 2 and 3 – Implemented adjustments.

	C_{10} [MPa]	C_{01} [MPa]
MR set 1	0.677	1.621
MR set 2	0.300	0.750
MR set 3	0.210	0.525

For the modelling of the index finger exoskeleton was used parabolic solid elements with a mesh size of 2.5 mm and a fixed constraint was applied on the surface corresponding to the base of the hand (Figure 5.4). The simulation was repeated six times (six forces) for each set of parameters, and then the values were compared with the average experimental tests.

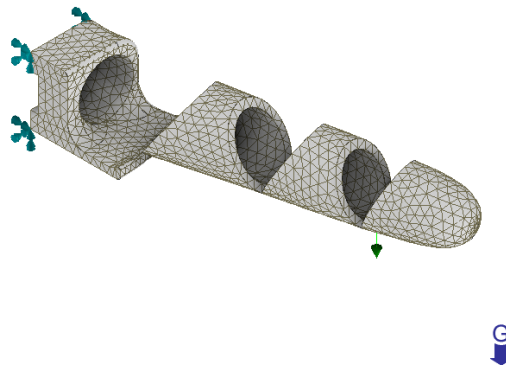


Figure 5.4. Modelling of index finger exoskeleton in Autodesk Inventor Nastran®. Fixed constraint, applied force and gravity.

The analysis of Figure 5.5 allows to conclude that using the “MR set 1” parameters, the predicted vertical displacement is lower than the experimental one. This means that the stiffness of the finger modelled with this set of parameters is larger than the stiffness measured experimentally. So, the value of the parameters was decreased (“MR set 2”) in order to reduce the stiffness of the finger in the numerical model. Using the new set of material parameters (“MR set 2”) in the numerical simulations allows to conclude that the

predicted vertical displacements were closer to the experimental ones. However, there was still a significant difference for own weight, 0.07 N and 0.16 N. Therefore, a decrease in the parameters was made (“MR set 3”) and the variations between simulation and experimental were significantly reduced. The numerical values became slightly less rigid than the experimental ones, except when only the own weight is applied. The discrepancy between the vertical displacement of the own weight, about 6.5 mm, can be explained by the inexistence of loads or lower loads that lead to larger measurement errors. However, as the aim is to simulate the finger with different pressures, gravity becomes irrelevant.

The difference between the numerical average obtained with the set of parameters “MR set 3” and the experimental results average is lower than 0.18 %, allowing to conclude that the model is accurate and could be used in the simulation of the exoskeleton and the fibre-reinforced actuator assembly.

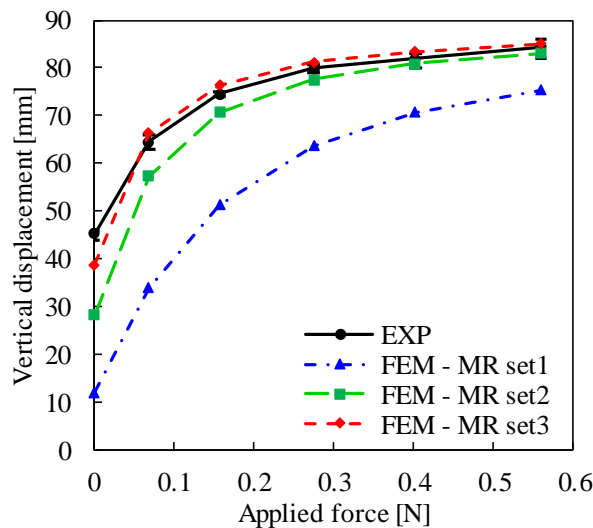


Figure 5.5. Vertical displacement for each force applied. Comparison of experimental tests and 3 different types of FEM (MR set 1, MR set 2 and MR set 3.)

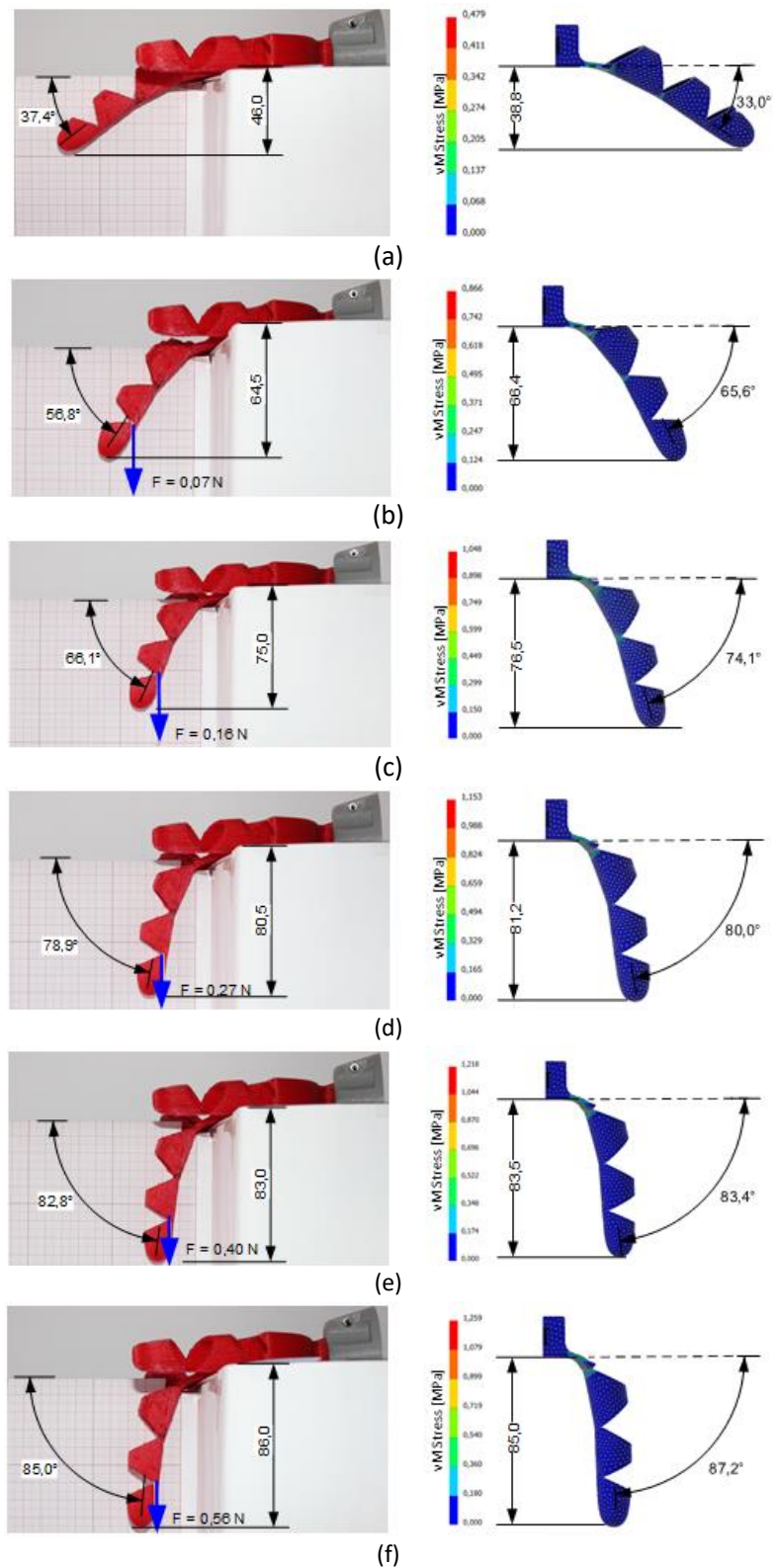


Figure 5.6. Vertical displacements of the index finger exoskeleton and the maximum deflection value from the tip of the finger to the bottom surface of the hand (degrees). All displacements values in mm. Left-side: experimental tests and right-side: FEM - MR set 3 with the results in von Mises Stress [MPa]. Forced applied: (a) Own weight (b) 0.07 N (c) 0.16 N (d) 0.27 N (e) 0.40 N (f) 0.56 N.

5.2.2. Fibre-Reinforced Actuator

As mentioned in section 3.2, the actuator is composed of Ecoflex™ 00-50 and a PET reinforcement, that consists of a high stiffness material with a very high modulus of elasticity and due to its winding shape, the actuator does not exhibit radial deformations, providing only longitudinal deformation, which consequently increases the length of the actuator. To explain the relevance of the reinforcement, a numerical simulation of an actuator without reinforcement was created in order to help the reader to interpret its function (Figure 5.7(a)). It can be observed that when the reinforcement is not used, the actuator tends to deform radially creating a balloon shape. On the other hand, the inclusion of the PET reinforcement, leads to an increase of the actuator length as the interior pressure increases (Figure 5.7(b)).

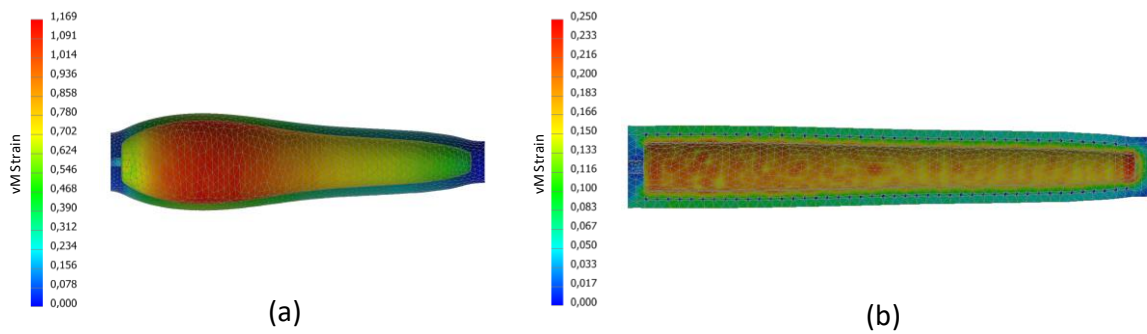


Figure 5.7. Pressurized actuator modelling without reinforcement (a) and with reinforcement (b). Both models pressurized with 30 kPa. Von Mises Strain results.

In order to assess the accuracy of the material parameters used in [49] for the mechanical characterization of the Ecoflex™ 00-50 with the Ogden model, the numerical results of the actuator (without being inserted in the exoskeleton) are compared with the experimental ones. The objective was to obtain the increase of length (maximum value of horizontal displacement) for different pressures and compare the range of discrepancy between them and apply the necessary adjustments to the parameters that describe the model.

The experimental tests were performed for pressures of 20, 40, 50 and 60 kPa. To provide better visualization of the horizontal displacement and to obtain a better precision of the results, a millimetre sheet of paper was placed under the actuator, and a part was created in the 3D printer to fix the actuator base (zone where the actuator fits into the exoskeleton) to guarantee always the same initial reference of the actuator (Figure 5.12). The part was fixed with two screws to a wooden board placed under the sheet of paper. Similarly,

to Ninjaflex material, the experimental tests were repeated three times for each pressure, and then the average was made (Table 5.6).

Table 5.6. Results of maximum horizontal displacement for the respective pressures. Three experimental tests and the average for each pressure.

Pressure (kPa)	Maximum Horizontal Displacement (mm)			
	EXP1	EXP2	EXP3	$\overline{\text{EXP}}$
20.0	5.0	5.5	5.0	5.17
40.0	12.0	12.5	12.0	12.17
50.0	16.0	15.5	16.5	16.00
60.0	23.0	22.5	23.5	23.00

Regarding the FEM simulations, the parameters used to characterize the Ecoflex™ 00-50 model are listed in Table 5.7. The first set of parameters (FEM- Ogden set 1) are the study parameters [49], as mentioned previously, and the next two sets of parameters (FEM- Ogden set 2 and 3) are improvements that were necessary to approximate the experimental results. All models used the value $D = 1 \times 10^5$. For the mechanical properties of the reinforcement they are obtained directly from the materials library that *Autodesk Inventor* provides ($\rho = 1541 \text{ kg/m}^3$; $E = 2.76 \times 10^9 \text{ Pa}$; $\nu = 0.417$; $\sigma_s = 5.51 \times 10^9 \text{ Pa}$; $\sigma_y = 5.44 \times 10^9 \text{ Pa}$).

Table 5.7. Ogden parameter values for Ecoflex™ 00-50. FEM-Ogden set 1 – parameters obtained for bibliographic review. FEM Ogden set 2 and 3 – improvements to achieve a characterization closer to the experimental.

Parameter set	Parameter values [MPa]		Incompressible value
FEM – Ogden set 1	$\alpha_1 = 1.55$ $\alpha_2 = 7.86$ $\alpha_3 = -1.91$	$\mu_1 = 107900$ $\mu_2 = 21.47$ $\mu_3 = -87100$	$D_1 = 1 \times 10^5$
FEM – Ogden set 2	$\alpha_1 = 1.05$ $\alpha_2 = 4$ $\alpha_3 = -1.6$	$\mu_1 = 1.5 \times 10^5$ $\mu_2 = 60$ $\mu_3 = -1300$	$D_1 = 1 \times 10^5$
FEM – Ogden set 3	$\alpha_1 = 1.05$ $\alpha_2 = 4$ $\alpha_3 = -1.6$	$\mu_1 = 1.125 \times 10^5$ $\mu_2 = 45$ $\mu_3 = -975$	$D_1 = 1 \times 10^5$

Two simplifications have been made in the finite element model to reduce the computational cost. The design of the PET reinforcement was not modelled with the same geometry of the experimental reinforcement because the diameter of the experimental reinforcement is smaller than the dimensions of the remaining actuator. This diameter required tiny finite elements that made the convergence of the solution difficult and

increased the time of the simulations dramatically. However, by increasing the dimensions of the reinforcement and changing the shape to a square transversal section, the stiffness of the model also increased, becoming different from reality. The solution to this problem was to decrease the number of reinforcements turns. Beyond the geometry, the experimental reinforcement consists of a continuously coiled thread, while numerically the reinforcement is composed by rings placed with a specific spacing between them (Figure 5.8).

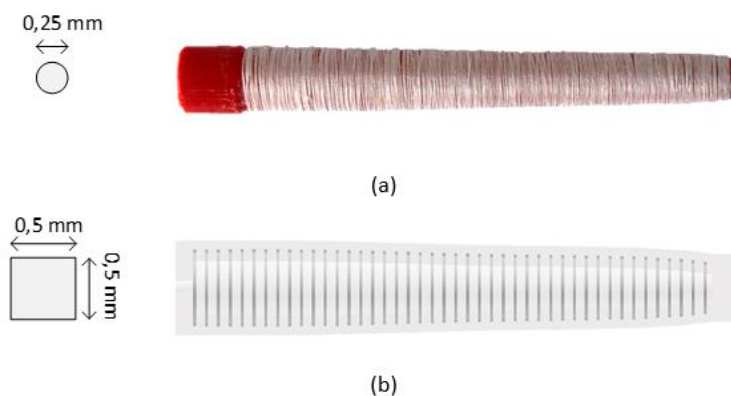


Figure 5.8. First simplification. Real vs Numerical PET reinforcement geometry. (a) Cylindrical cross-section with 0,25 mm diameter; (b) Square cross-section with 0,5 mm width (44 rings).

The second assumption is related with the constrains. Experimentally the base of the actuator has created with two PLA parts to seal the chamber and help to adjust the fitting into the exoskeleton hole. These parts inserted in the exoskeleton hole enable the actuator to be fixed. Numerically, a fixed constraint in the base was assigned, and only Ecoflex™ 00-50 (without 3D parts) was used.

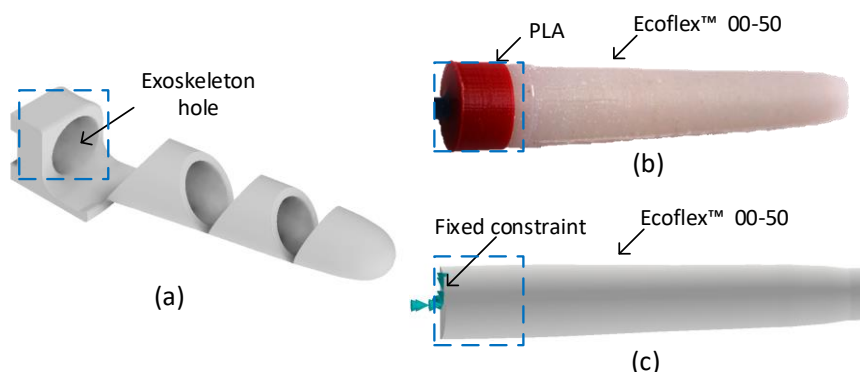


Figure 5.9. Second simplification. (a) Illustration of the exoskeleton hole area; (b) Experimental actuator base; (c) FEM actuator base.

The parabolic (quadratic) solid tetrahedral elements were used for both materials, with a mesh size of 1 mm and 1,5 mm, for the reinforcement and the Ecoflex™

00-50, respectively. The pressure was applied to the inner surfaces of the chamber with the same values mentioned in the experimental tests. Moreover, to reduce the simulation time, the actuator was split in the middle and applied a half-symmetric constraint.

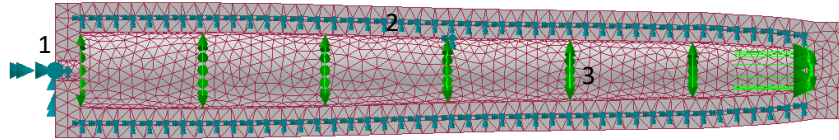


Figure 5.10. FEM Model development. 1 – Fixed constraint; 2 – Half-symmetric constraint; 3 – Internal pressure.

As the reinforcement is inside the silicone and a casting process manufactured the assembly, the contact surface assigned to the various rings of the reinforcement facing the Ecoflex™ 00-50 was the *bonded* type. This type of contact does not allow the separation of the components or even relative movement between them. The model has 44 rings, and each ring has 4 contact surfaces connected to the silicone, consequently there are 176 contacts. Possibly in the experimental actuator exists some relative movement between reinforcement and silicone; however, it would be an insignificant value since the longitudinal deformation mostly occurs in the areas between the rings and not in the ring area itself. Thus, the attribution of this type of contact was very close to reality and eliminated several convergence problems compared to other contact models. Concerning the choice of *master* and *slave* surfaces, *Nastran*® software advises inserting as master the surfaces with a coarser mesh. However, when the mesh of both surfaces is similar, it is advised to assign the master to the stiffer surface. Thus, the reinforcement was considered the master entity and the Ecoflex™ 00-50 the slave entity. In the *Nastran*® software, the contact surfaces only occur between the nodes of one surface and the elements of another surface, where the *slave* entity uses the nodes and the *master* entity the elements. That means the contact surface is only detected if the *slave* nodes are in contact with the elements of the *master*. This type of penetration is called *unsymmetric* contact. Another option is the *symmetric* contact. In this contact, it does not matter which is the *master* and *slave* surface because there is the change of the entity of the surfaces, i.e. the same surface will be once *master* and another *slave*. The *symmetric* contact option is the safest; however, as it contains more contact elements, the analysis is slower and requires more computational memory. For the *stiffness factor* used in the penalty method (contact enforcement), no value has been entered, so the default program puts the value of 1.

For each set of Ecoflex™ 00-50 parameters, the simulation was repeated four times (20, 40, 50 and 60 kPa), and the results were inserted in Figure 5.11. For the first set of parameters (FEM – Ogden set 1), the predicted maximum horizontal displacements were considerably lower than the results obtained experimentally, meaning that the characterization of the material numerically provides more rigidity. One of the reasons for this difference lies not in using the vacuum chamber when manufacturing the actuator, allowing the external environment to create air bubbles in the silicone, reducing its stiffness. To approximate the experimental results, the parameters were decreased slightly (FEM – Ogden set 2) in order to lower the stress-strain curve. The simulations were again performed, and it was concluded that the stiffness of the material numerically was still higher, being necessary to lower the parameters again (FEM – Ogden set 3). After new simulations, it was possible to conclude that this last set of parameters presents horizontal displacement values close to the experimental one, with an error of less than 10 % up to 50 kPa, determining these parameters acceptable. For the value of 60 kPa, a significant discrepancy (17.6 %) is noted that can be explained by the experimental result beginning to show some folding due to the complexity of placing the symmetrical reinforcement manually (Figure 5.12(d)).

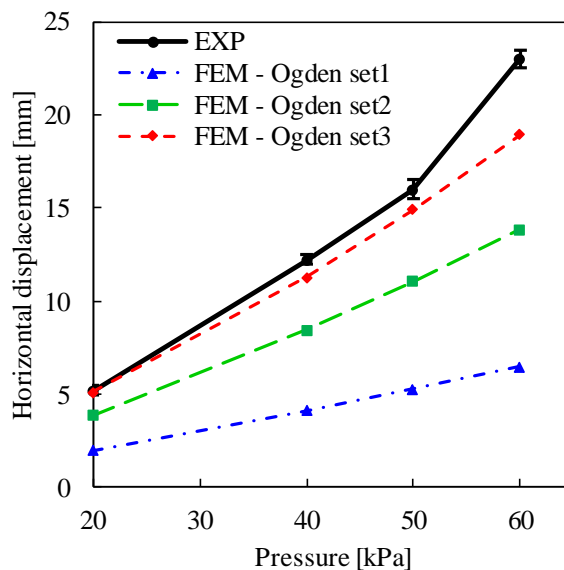


Figure 5.11. Horizontal displacement for each force applied. Comparison of experimental tests and 3 different types of FEM (Ogden set 1, Ogden set 2 and Ogden set 3).

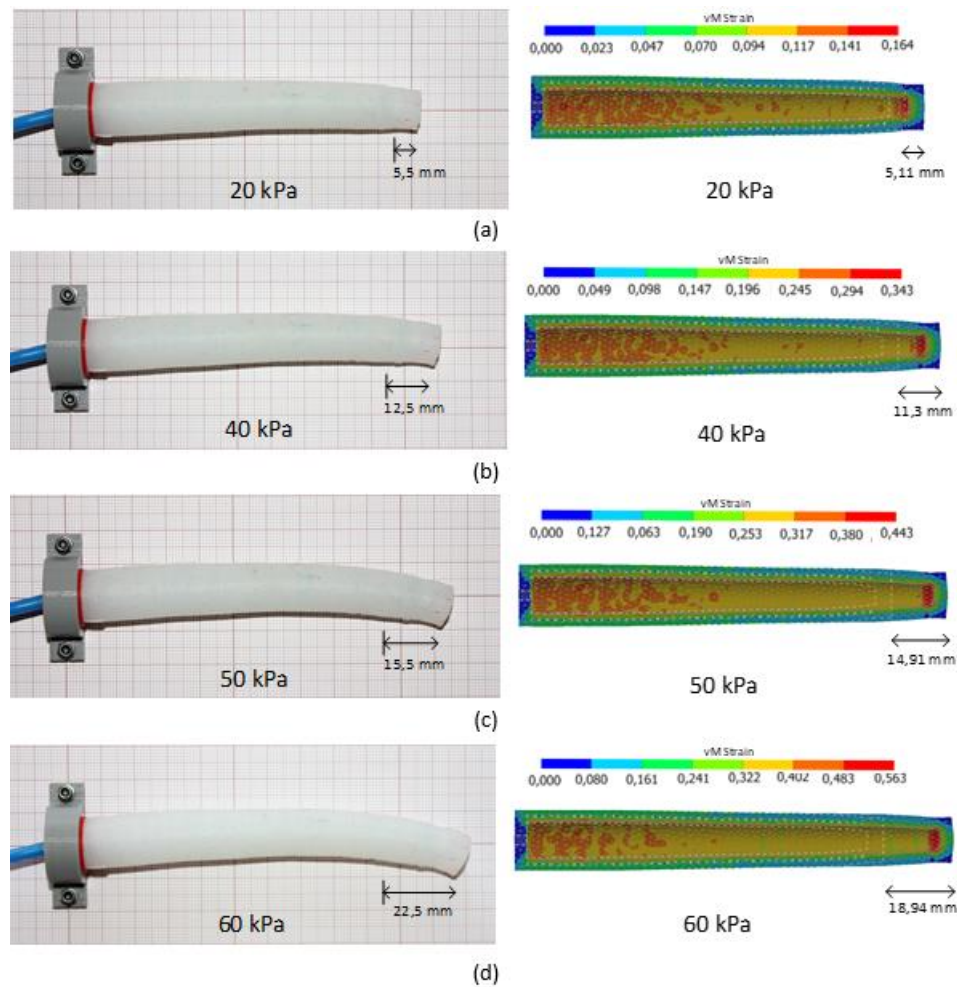


Figure 5.12. Fibre-reinforced actuator test. Left-side: experimental tests (EXP2) and right-side: FEM simulations with von Mises Strain results (FEM- Ogden set 3). (a) 20 kPa; (b) 40 kPa; (c) 50 kPa; (d) 60 kPa.

From the visualization of the results of Figure 5.12, it is noticeable that the reinforcement shows little strain, being able to restrict the radial deformation of the internal layer of the actuator. Also, it is visible that the leftmost area of the inner chamber of the actuator has higher von Mises strain values. These are justified by the larger internal diameter of this zone which in turn increases the surface area. However, the area with the highest von Mises strain value is located in a minimal surface area (actuator tip), which is justified by the non-existence of reinforcement to prevent it. It was concluded that with the increase in pressure, the horizontal displacement increases and could reach values very close to the experimental ones. Furthermore, there is no increase in the diameter of the actuator and can be concluded that the behaviour is quite similar to the experimental one.

5.2.3. Assembly - (Exoskeleton and Fibre-Reinforced Actuator)

After a detailed behaviour analysis of the two separate parts that ensured a better performance of the materials, the assembly was then simulated. The fibre-reinforced actuator was inserted into the index finger exoskeleton, and afterwards, the experimental tests and the numerical modelling was performed.

Firstly, in the experimental tests, the hand was positioned in the same way as the experimental exoskeleton tests (section 5.2.1). Then, the actuator was pressurized with different pressure values (20, 30, 40, 50 and 60 kPa), which consequently causes the folding of the finger, and the maximum vertical displacement was evaluated (Table 5.8).

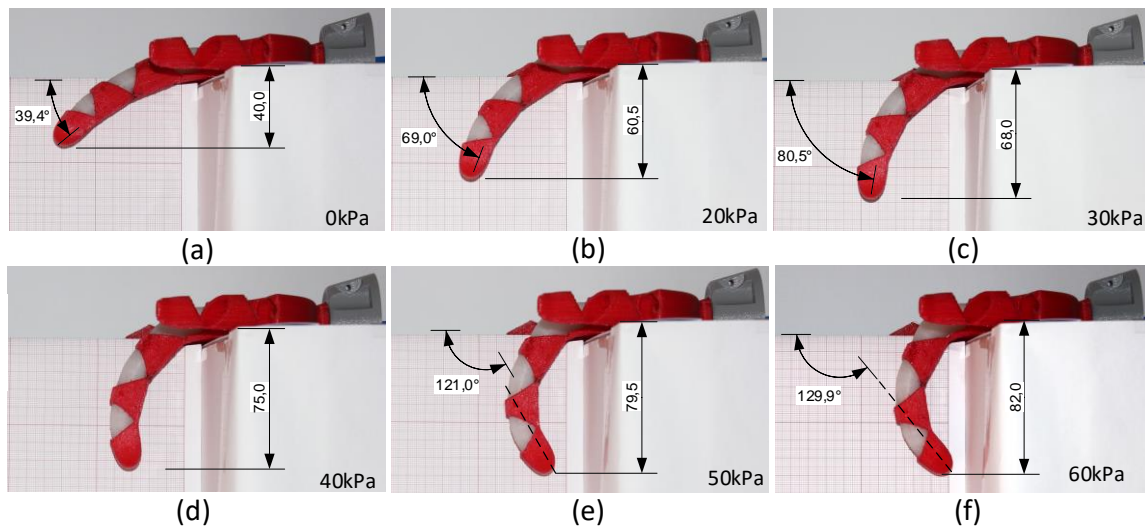


Figure 5.13. Experimental results of the index finger. Vertical displacement results of EXP3. All displacements are in mm.

Table 5.8. Results of maximum vertical displacement for the respective pressures. Three experimental tests and the average for each pressure.

Pressure (kPa)	Maximum Vertical Displacement (mm)			
	EXP1	EXP2	EXP3	$\overline{\text{EXP}}$
0.0	38.5	40.0	40.0	39.50
20.0	61.0	60.5	60.5	60.67
30.0	69.0	68.5	68.0	68.50
40.0	74.0	75.0	75.0	74.67
50.0	79.0	80.0	79.5	79.50
60.0	81.5	81.5	82.0	81.67

Secondly, in the FEM simulations, the parameters used to characterize the materials' models were those that presented most similarity with the previous experimental results:

- Ninjaflex – FEM MR set 3;
- Ecoflex™ 00-50 – FEM Ogden set 3;
- PET reinforcement – *Autodesk Inventor Nastran*® properties;

The mesh size of the reinforcement and the actuator was the same used in the last model with 1mm and 1,5 mm, respectively. For the exoskeleton, the mesh size was decreased to 1,5 mm to enhance the performance of the model convergence. All of them are modelled as parabolic solid elements. A fixed constraint was applied in the base of the exoskeleton, and just like the fibre-reinforced actuator model, the assembly was split in the middle and was implemented a half-symmetric constraint. The pressure was again applied on the inner surfaces of the actuator. The gravity was not applied to the model because the hand could have been actuated in several asymmetric positions, creating a discrepancy where a few positions were more favoured than others. Besides that, the own weight would be practically insignificant compared to the internal pressures that the actuator is subject.

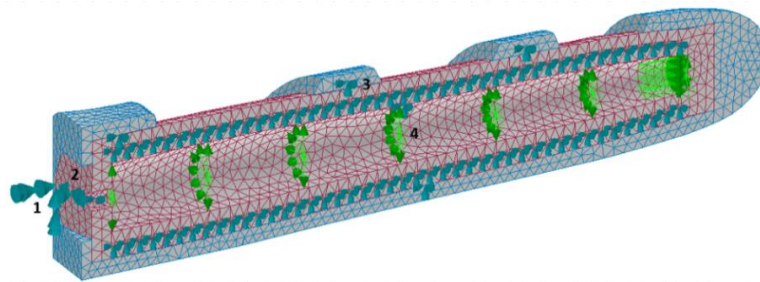


Figure 5.14. FEM model development. 1 – Fixed constraint; 2 – Ty constraint; 3 – Half-symmetric constraint; 4 – Internal pressure.

Concerning the contact surfaces assigned in the previous simulation between the reinforcement and the actuator have been repeated for this new model, being added the contact surfaces between actuator and exoskeleton. Ideally, the contact surfaces between them should be separated in all contacts, but this type of contact presents much complexity, increasing the time and the difficulty to converge. For this purpose, some simplifications were created in order to try to find a solution very similar to reality and simultaneously to reduce the simulation time and the convergence problems. In Figure 5.15 are visible the 10 contacts applied between the exoskeleton and the actuator. For contact number 1, the *sliding/no separation* contact was chosen because although the actuator is inserted in the exoskeleton and there is no separation, the actuator has the capacity to deform longitudinally when subjected to pressure, needing to slide relative to the exoskeleton. Next, when the pressure inserted in the actuator increases, there is experimentally a clear separation in the

bottom region of the actuator (palm side), so the surfaces 2, 3, 5 and 7 need the separation contact. The reason for the existence of contact surfaces 4 and 6 are justified by the lack of convergence of the model when surfaces 3 and 5 comprise 4 and 6. Therefore the sliding/no separation contact type has been placed on these two surfaces allowing an excellent approximation to reality because experimentally the actuator in these areas only has slid. On surfaces 8 and 9 the sliding/no separation type has been placed again because in this area the actuator does not tend to separate but rather to slide. The justification for being two separate surfaces with the same type of contact is due to a readjustment of the mesh, which improved the convergence of the model. Finally, contact number 10 corresponds to the tip of the actuator, i.e. one of the zones with the highest contact pressure between surfaces, which induces that the type of bonded contact was a good approximation. However, with the attempt to assign this sliding/no separation contact, it was observed that there is a slight sliding of the actuator in a direction opposite to the palm of the hand. In all contacts, the value of the stiffness factor corresponds to 1 (default). Some areas show in the results a certain penetration, which indicates that the value of the factor should be increased. However, the increase in value of the *stiffness* factor leads to convergence problems in the model.

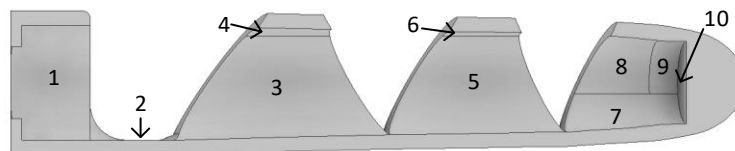


Figure 5.15. Contact surfaces between the exoskeleton and the actuator. (1), (4), (6), (8), (9), (10) – Sliding/no separation; (2), (3), (5), (7) – Separation.

After the results were obtained, it was seen that the finger folding was much lower than the experimental value. In order to improve the convergence of the model and the folding results, several attempts have been made. When the incompressibility value of Ecoflex™ 00-50 was changed, it was noted that for the same pressures, the lower its value, the greater the fold. Also, the reduction of the D value made it possible to achieve higher pressures without problems of convergence (and consequently more fold). To check the coherence of the value change, at the same time that the value was changed in the assembly simulation, it was also changed in the fibre-reinforced actuator simulation. While in the

assembly, the simulation was closer to the real one, in the fibre-reinforced actuator simulation, a very different deformation from the real one started to appear (Figure 5.16).

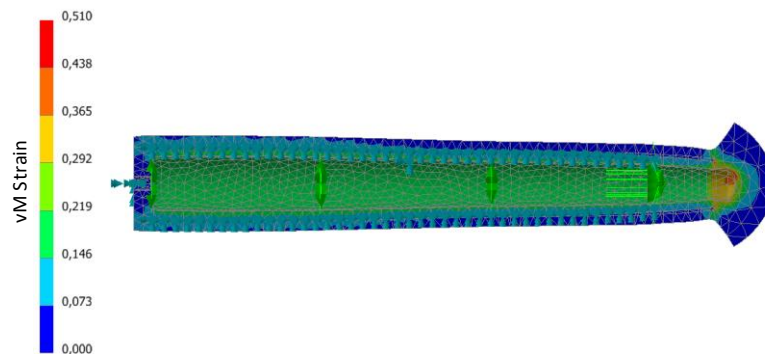


Figure 5.16. FEM simulation of a fibre-reinforced actuator with $D=10$. (20 kPa)

By noting this incongruence, it was concluded that since D controls the volume variation of a material when subjected to a load, if the actuator is more constrained (on the assembly), its effect is less visible. Thus, the value of D has been reduced from 1×10^5 to 10. Based on the same approach, considering that the Poisson coefficient measures the transverse deformation of isotropic material and considering that the reinforcement is restricted by silicone, the value of the Poisson coefficient has been decreased from 0.417 to 0.17. A value below 0.17 would not be realistic.

Experimentally the finger reached its maximum folding angle at 100 kPa (fingertip next to palm), but numerically, it was only possible to obtain results up to 47 kPa. One possible reason for the model not being able to converge might be because a particular increment changes the shape of the model significantly. However, the model was computed with 200 and 300 increments, to decrease the value of the pressure in each increment, which consequently, decreased the model shape, but in both cases, it did not improve the convergence. The highest result was obtained with 100 increments.

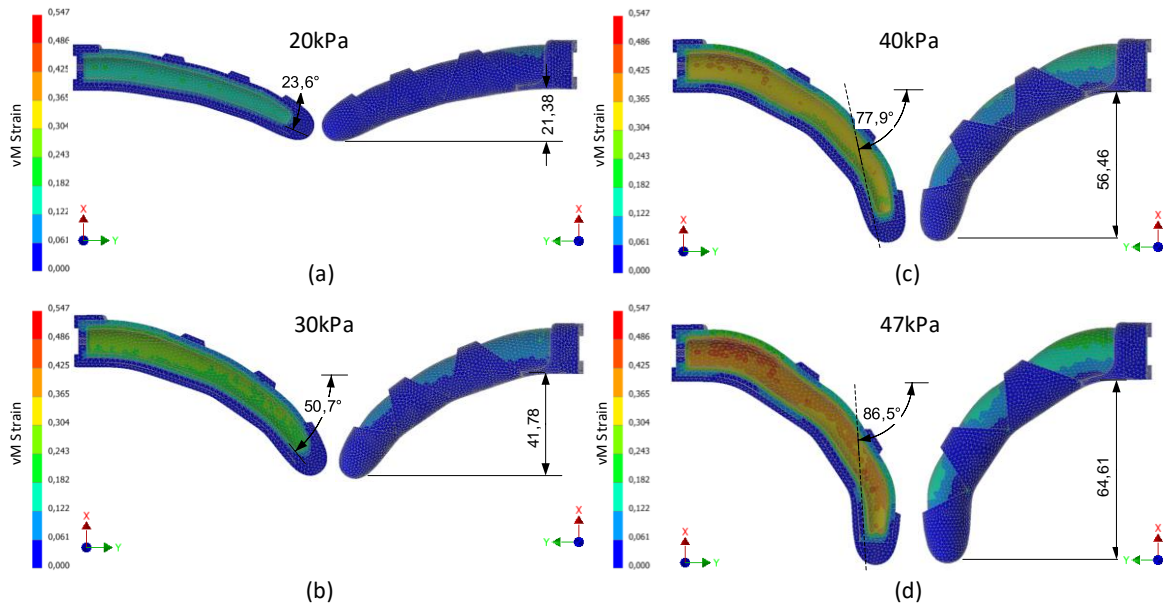


Figure 5.17. FEM results of the assembly (Exoskeleton + Fibre-reinforced actuator). Visualization of von Mises Strain results, vertical displacement and folding angle. All displacement values are in mm. (a) 20 kPa; (b) 30 kPa; (c) 40 kPa; (d) 47 kPa.

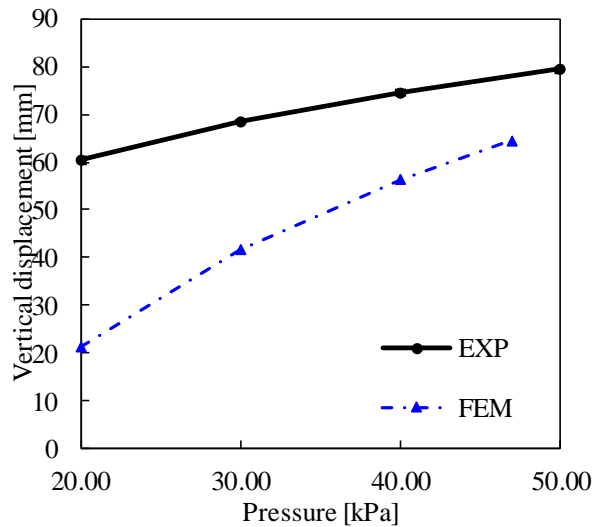


Figure 5.18. Vertical displacement for each pressure applied. Comparison between experimental tests and FEM simulations.

The numerical results show lower vertical displacement values compared to the experimental ones, i.e. less bending for the same pressure. But it can be seen that with the increase in pressure the numerical result tends to approach the experimental value. For the pressure of 40 kPa there is a difference between the numerical and the experimental of 24.34%, which continues to decrease until the numerical convergence fails. Despite the

results discrepancy, it is possible to visualize (Figure 5.17) that the finger folding behaviour is similar to the experimental one (Figure 5.13), following the same evolution.

5.2.4. Finger Force Test

The maximum fingertip force is a relevant characteristic in the application of object handling tasks, being one of the main direct relations with the weight of objects that a finger can withstand. So, it was determined experimentally and numerically.

Experimentally, the determination of the force was realised with a balance machine (TechMaster ES-3000A) (Figure 5.19(a)). A support was created that fixes the hand in the horizontal at a vertical distance of 40 mm between the palm side and the balance. The height has been chosen in order to assure that the finger has a bend lesser than 45 degrees so that the force component can be mostly vertical. Moreover, at the same time the value should be above zero degrees because this setting is not useful when handling objects. The index finger is then pressurized (constant pressure increases), and when the fingertip starts to touch the balance, it starts to register its mass. The value of the maximum mass displayed multiplied by the acceleration of gravity corresponds to the maximum value of the finger's pressure force.

Numerically, a duplicate of the assembly model (Section 5.2.3) was executed, with a rigid body having been added with the respective distances described in the experimental tests. The rigid body replaces the experimental balance. When the simulation finished, the reaction force was obtained in the area of the constraint of the rigid body, which indicates the value of the maximum force that the fingertip has applied to the rigid body. For the value of the reaction force, it was necessary to multiply by two, because the finger model was divided in half.

The values of the fingertip forces obtained experimentally and numerically have been inserted in Figure 5.20. For the experimental tests, pressures from 20 to 80 kPa (with an interval of 10 kPa) were applied. Numerically, the fingertip only reaches the surface at 33 kPa, so the results were obtained for pressures of 35, 40, 45 and 46.5 kPa. From the latter value, the model once again failed to converge. The maximum fingertip force value corresponds to 0.81 N for the maximum pressure reached of 80 kPa. While numerically, the maximum force value corresponds to 0.176 N for the 47 kPa pressure. The numerical results show some discrepancy with the experimental, but both exhibit the same trend. As pressure

increases, the fingertip force tends to increase linearly. Part of this difference can be explained by the absence of the force of gravity in the numerical model.

Overall the fingertip force experimental results indicate relatively low values, with two causes being identified. The first is that the fingertip has a specific angle to the surface of the balance, whereby the maximum finger force component will also have a specific angle, while the balance only measures the vertical component. The second, the pressure value was only executed up to 80 kPa because it was verified that the actuator started to make an unexpected deformation by having an obstacle in front. Therefore, this force value may not represent the maximum force value reached by the finger, being possibly able to reach higher values with higher pressures for a larger finger bending angle (without the balance).

Finally, it should be noted that the total force of the hand consists of the sum of the five fingers.

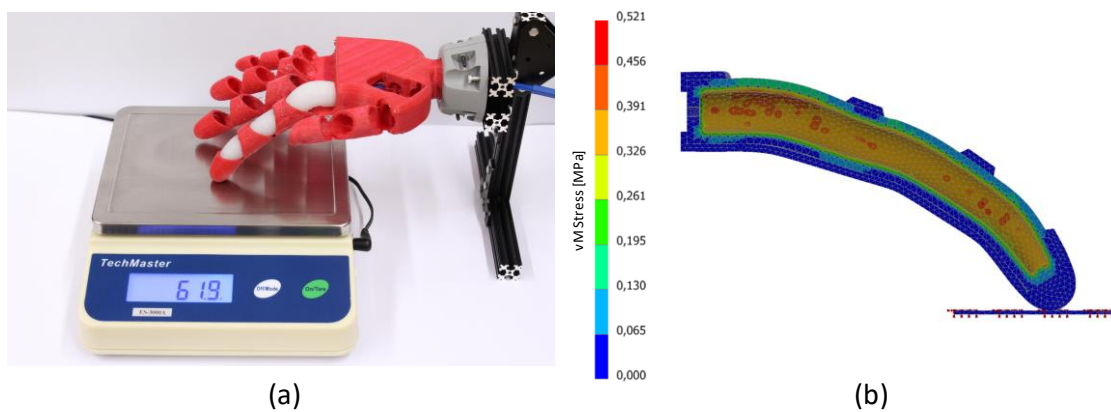


Figure 5.19. Determination of the maximum fingertip force. (a) Experimental test for 60 kPa; (b) FEM simulation for 46,5 kPa.

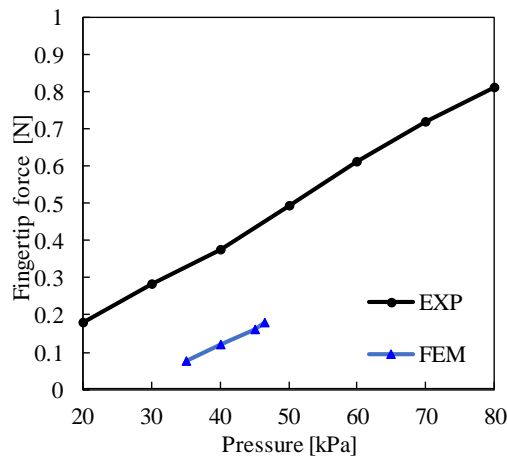


Figure 5.20. EXP and FEM results of maximum fingertip pressure force.

6. CONCLUSIONS

This dissertation describes the design and manufacture of a pneumatic robotic hand prototype which is based on the robotics sub-area soft robotics. Soft materials were used, i.e. materials with elastic, flexible and soft properties, which provides to the robotic hand the ability of adaptation to the environment in a safe way and with the necessary compliance to deal with delicate objects. The soft hand offers a human-like shape, with the dimensions of an adult human hand.

The concept of the hand motion was based on the article of Jan Fras and Kaspar Althoefer [3][30], where the hand was built by two different types of components, the exoskeleton and the reinforced actuators. The first component was created from direct 3D printing using a TPE called Ninjaflex. Overall the 3D printed material provided good quality and precision to the robotic hand, except to the palm of the hand in the area where the two actuators would be inserted to create the opposition/reposition movement. This zone became more rigid than supposed, however, the problem was not directly related to the 3D printing, but to the CAD design. For the actuators a manual deposition process was used, pin casting, where the moulds and pins (cores) were created in 3D printing and the material cast in the moulds consisted of the Ecoflex™ 00-50, an elastomer with excellent elongation properties, elasticity and low hardness. These actuators also include a polyethylene terephthalate thread as a reinforcement function to avoid radial deformations and favour longitudinal deformations. In addition, to seal the actuators, two 3D printed PLA parts were created, which were glued to the base of the actuator (inlet pressure area). The created actuators showed good reliability and resistance for the required pressure range; however, the construction process required a lot of manual care, being necessary to repeat them a few times to achieve good results due to the porosity during deposition and cure. In the assembly, when the actuators were pressurized, the finger motion demonstrated good bending motion.

Then, a numerical model was developed with *Autodesk Inventor Nastran*® software in order to compare the folding behaviour of the index finger with the experimental tests. The objective of the model elaboration was to try to approximate the numerical results with the experimental ones, because once these are proved, it means that the model can

perform the same concept for different geometries and optimizations. The Ninjaflex and Ecoflex™ 00-50 are considered hyperelastic materials, their properties are obtained from the literature. To ensure a good material characterization, it was decided to model the components separately first, and compare the mechanical behaviour with the experimental tests. For the exoskeleton, tests with suspended weights at the fingertip were executed, where the vertical displacement was noted. For the reinforced actuators, tests of free horizontal displacement with different inlet pressures were executed. In both cases, the numerical characterization revealed stiffness values higher than the experimental results, so adjustments in the parameters were performed to obtain acceptable values. After the necessary adjustments, the assembly model was created. However, due to the geometry complexity, and because the model contains three different materials, there were many difficulties. It was possible to observe that the mechanical behaviour follows the same trend line, but with the need for higher-pressure values to achieve the same experimental results. Also, numerical results were not achieved after a value above 47 kPa. One of the reasons that may justify the lack of convergence is due to a specific increment in the model that strongly changes the bending behaviour of the finger.

Finally, a fingertip force test was also performed, because it is a very important characteristic in the handling of objects. The hand was positioned at 40 mm vertical displacement between the palm and the fingertip. Although the numerical results show discrepancy with the experimental, both show the same trend with increasing pressure.

6.1. Future Work

Given the good results of the exoskeleton printed directly with a 3D printer with a TPE material, direct manufacture of the actuators could also be an excellent choice. As referred in state of the art, there are already works developed to 3D print silicones directly, designated as DIW; however, it is a process that needs to make big changes in the 3D printer. Recently, Recreus launched a new TPE (Filaflex 70A)[50], which is described as ultra-soft, flexible and with 900% elongation. As the hardness of this material is less than the one presented by Ninjaflex, it means that Ninjaflex is able to restrict actuator deformation at the desired locations and perform good bending behaviour. Besides that, this material has higher

hardness than Ecoflex™ 00-50, the stiffness of the set increased, and the hand was able to withstand higher forces.

Concerning manufacturing, since the palm of the hand presents excessive stiffness in the thumb area limiting its opposition/reposition movement, a design improvement will be created.

The hand will incorporate a high precision pneumatic control system, to execute different grasping postures.

Regarding to numerical modelling, the problem of lack of convergence will be studied again, and when solved, different variations of geometry will be performed to study their influence on finger bending.

BIBLIOGRAPHY

- [1] D. Trivedi, C. D. Rahn, W. M. Kier, and I. D. Walker, “Soft robotics: Biological inspiration, state of the art, and future research,” *Appl. Bionics Biomech.*, vol. 5, no. 3, pp. 99–117, 2008, doi: 10.1080/11762320802557865.
- [2] F. Putzu, J. Konstantinova, and K. Althoefer, “Soft Particles for Granular Jamming,” pp. 65–74, 2019, doi: 10.1007/978-3-030-25332-5_6.
- [3] J. Frasn and K. Althoefer, “Soft Biomimetic Prosthetic Hand: Design, Manufacturing and Preliminary Examination,” *IEEE Int. Conf. Intell. Robot. Syst.*, pp. 6998–7003, 2018, doi: 10.1109/IROS.2018.8593666.
- [4] C. Laschi, M. Cianchetti, B. Mazzolai, L. Margheri, M. Follador, and P. Dario, “Soft robot arm inspired by the octopus,” *Adv. Robot.*, vol. 26, no. 7, pp. 709–727, 2012, doi: 10.1163/156855312X626343.
- [5] P. M. Matos, “Collaborative Gripper for Robotic Application.” Tese de Mestrado em Engenharia Mecânica na especialidade de Produção e Projeto, Departamento de Engenharia Mecânica, Faculdade de Ciências e Tecnologia, Universidade de Coimbra, 2019.
- [6] R. Deimel and O. Brock, “A Novel Type of Compliant, Underactuated Robotic Hand for Dexterous Grasping,” 2015, doi: 10.15607/rss.2014.x.018.
- [7] D. Rus and M. T. Tolley, “Design, fabrication and control of soft robots,” *Nature*, vol. 521, no. 7553, pp. 467–475, 2015, doi: 10.1038/nature14543.
- [8] C. P. Chou and B. Hannaford, “Measurement and modeling of McKibben pneumatic artificial muscles,” *IEEE Trans. Robot. Autom.*, vol. 12, no. 1, pp. 90–102, 1996, doi: 10.1109/70.481753.
- [9] A. D. Marchese, R. K. Katzschmann, and D. Rus, “A recipe for soft fluidic elastomer robots,” *Soft Robot.*, vol. 2, no. 1, pp. 7–25, 2015, doi: 10.1089/soro.2014.0022.
- [10] B. Mosadegh *et al.*, “Pneumatic networks for soft robotics that actuate rapidly,” *Adv. Funct. Mater.*, vol. 24, no. 15, pp. 2163–2170, 2014, doi: 10.1002/adfm.201303288.
- [11] K. C. Galloway, P. Polygerinos, C. J. Walsh, and R. J. Wood, “Mechanically Programmable Bend Radius for Fiber-Reinforced Soft Actuators,” *Appl. Phys. B Lasers Opt.*, vol. 105, no. 4, 2011, doi: 10.1109/ICAR.2013.6766586.
- [12] H. Wang *et al.*, “Fiber-reinforced soft robotic anthropomorphic finger,” *2016 Int. Conf. Robot. Autom. Eng. ICRAE 2016*, pp. 1–5, 2016, doi: 10.1109/ICRAE.2016.7738777.
- [13] J. Frasn and K. Althoefer, “Soft Fiber-Reinforced Pneumatic Actuator Design and

- Fabrication: Towards Robust, Soft Robotic Systems,” *Lect. Notes Comput. Sci. (including Subser. Lect. Notes Artif. Intell. Lect. Notes Bioinformatics)*, vol. 11649 LNAI, pp. 103–114, 2019, doi: 10.1007/978-3-030-23807-0_9.
- [14] Y. Li, Y. Chen, Y. Yang, and Y. Wei, “Passive Particle Jamming and Its Stiffening of Soft Robotic Grippers,” *IEEE Trans. Robot.*, vol. 33, no. 2, pp. 446–455, 2017.
- [15] Y. Li, Y. Chen, and Y. Li, “Distributed design of passive particle jamming based soft grippers,” *2018 IEEE Int. Conf. Soft Robot. RoboSoft 2018*, pp. 547–552, 2018, doi: 10.1109/ROBOSOFT.2018.8405383.
- [16] M. Elkeran and M. Fanni, “A transient FEA-based methodology for designing soft surgical manipulators,” in *Proceedings of 2018 IEEE International Conference on Mechatronics and Automation, ICMA 2018*, 2018, pp. 568–573, doi: 10.1109/ICMA.2018.8484508.
- [17] M. Cianchetti, T. Ranzani, G. Gerboni, I. De Falco, C. Laschi, and A. Menciassi, “STIFF-FLOP surgical manipulator: Mechanical design and experimental characterization of the single module,” *IEEE Int. Conf. Intell. Robot. Syst.*, no. August, pp. 3576–3581, 2013, doi: 10.1109/IROS.2013.6696866.
- [18] M. Cianchetti *et al.*, “Soft Robotics Technologies to Address Shortcomings in Today’s Minimally Invasive Surgery: The STIFF-FLOP Approach,” *Soft Robot.*, vol. 1, no. 2, pp. 122–131, 2014, doi: 10.1089/soro.2014.0001.
- [19] Z. Wang and S. Hirai, “A 3D printed soft gripper integrated with curvature sensor for studying soft grasping,” *SII 2016 - 2016 IEEE/SICE Int. Symp. Syst. Integr.*, pp. 629–633, 2017, doi: 10.1109/SII.2016.7844069.
- [20] Z. Wang, D. S. Chathuranga, and S. Hirai, “3D printed soft gripper for automatic lunch box packing,” *2016 IEEE Int. Conf. Robot. Biomimetics, ROBIO 2016*, pp. 503–508, 2016, doi: 10.1109/ROBIO.2016.7866372.
- [21] J. Fras, M. Macias, F. Czubaczynski, P. Salek, and J. Glowka, “Soft Flexible Gripper Design, Characterization and Application,” *Adv. Intell. Syst. Comput.*, vol. 543, pp. 368–377, 2017, doi: 10.1007/978-3-319-48923-0.
- [22] Y. Wang and Q. Xu, “Design and Fabrication of a Soft Robotic Manipulator Driven by Fiber-Reinforced Actuators,” *2018 IEEE Int. Conf. Mechatronics, Robot. Autom. ICMRA 2018*, pp. 157–161, 2018, doi: 10.1109/ICMRA.2018.8490539.
- [23] A. Hassan, H. Godaba, and K. Althoefer, “Design Analysis of a Fabric Based Lightweight Robotic Gripper,” *Lect. Notes Comput. Sci. (including Subser. Lect. Notes Artif. Intell. Lect. Notes Bioinformatics)*, vol. 11649 LNAI, pp. 16–27, 2019, doi: 10.1007/978-3-030-23807-0_2.
- [24] O. Pfaff, S. Simeonov, I. Cirovic, and P. Stano, “Application of finray effect approach for production process automation,” *Ann. DAAAM Proc. Int. DAAAM Symp.*, vol. 22, no. 1, pp. 1247–1248, 2011.
- [25] “MultiChoiceGripper.” [Online]. Available: https://www.festo.com/net/SupportPortal/Files/333986/Festo_MultiChoiceGripp

- er_en.pdf. [Accessed: 01-Apr-2020].
- [26] “Festo - Festo Media Service.” [Online]. Available: https://www.festo.com/net/en_group/SupportPortal/press.aspx?documentId=276499. [Accessed: 01-Apr-2020].
- [27] W. Crooks, G. Vukasin, M. O’Sullivan, W. Messner, and C. Rogers, “Fin Ray® effect inspired soft robotic gripper: From the robosoft grand challenge toward optimization,” *Front. Robot. AI*, vol. 3, no. NOV, pp. 1–9, 2016, doi: 10.3389/frobt.2016.00070.
- [28] P. Polygerinos, Z. Wang, K. C. Galloway, R. J. Wood, and C. J. Walsh, “Soft robotic glove for combined assistance and at-home rehabilitation,” *Rob. Auton. Syst.*, vol. 73, pp. 135–143, 2015, doi: 10.1016/j.robot.2014.08.014.
- [29] H. Zhao, K. O’Brien, S. Li, and R. F. Shepherd, “Optoelectronically innervated soft prosthetic hand via stretchable optical waveguides,” *Sci. Robot.*, vol. 1, no. 1, pp. 1–10, 2016, doi: 10.1126/scirobotics.aai7529.
- [30] J. Frasn and K. Althoefer, *Soft pneumatic prosthetic hand*, vol. 10965 LNAI. Springer International Publishing, 2018.
- [31] S. Walker, O. D. Yirmibeşoğlu, U. Daalkhajav, and Y. Mengüç, “Additive manufacturing of soft robots,” *Robot. Syst. Auton. Platforms*, pp. 335–359, 2019, doi: 10.1016/b978-0-08-102260-3.00014-7.
- [32] O. D. Yirmibesoglu *et al.*, “Direct 3D printing of silicone elastomer soft robots and their performance comparison with molded counterparts,” *2018 IEEE Int. Conf. Soft Robot. RoboSoft 2018*, pp. 295–302, 2018, doi: 10.1109/ROBOSOFT.2018.8404935.
- [33] H. K. Yap, H. Y. Ng, and C. H. Yeow, “High-Force Soft Printable Pneumatics for Soft Robotic Applications,” *Soft Robot.*, vol. 3, no. 3, pp. 144–158, 2016, doi: 10.1089/soro.2016.0030.
- [34] “What is FEA | Finite Element Analysis? — SimScale Documentation.” [Online]. Available: <https://www.simscale.com/docs/content/simwiki/fea/whatisfea.html>. [Accessed: 28-Mar-2020].
- [35] C. Duriez, “Control of elastic soft robots based on real-time finite element method,” *Proc. - IEEE Int. Conf. Robot. Autom.*, pp. 3982–3987, 2013, doi: 10.1109/ICRA.2013.6631138.
- [36] “SOFA – Tools for multi-material simulations.” [Online]. Available: <https://www.sofa-framework.org/applications/marketplace/tools-for-multi-material-simulations/>. [Accessed: 28-Mar-2020].
- [37] G. Agarwal, N. Besuchet, B. Audergon, and J. Paik, “Stretchable Materials for Robust Soft Actuators towards Assistive Wearable Devices,” *Sci. Rep.*, vol. 6, no. September, pp. 1–8, 2016, doi: 10.1038/srep34224.
- [38] A. B. Dawood, H. Godaba, and K. Althoefer, “Modelling of a Soft Sensor for Exteroception and Proprioception in a Pneumatically Actuated Soft Robot,” pp. 99–110, 2019, doi: 10.1007/978-3-030-25332-5_9.

- [39] B. E. P. Enes, “Actuation strategies for Underactuated Hands : Better Functionality & Better Anthropomorphism.” Master’s degree in Biomedical Engineering, Universidade of Coimbra, 2014.
- [40] J. G. A. Santos and M. Tavakoli, “Bio-inspired robotic gripper with hydrogel-silicone soft skin and 3D printed endoskeleton.” Master’s degree in Biomedical Engineering, Universidade of Coimbra, 2017.
- [41] “Pinterest.” [Online]. Available: https://www.pinterest.pt/pin/177821885262274082/?nic_v1=1aQDn0Xpw%2F%2BBoYco7%2BmzS9d36yw1ZDa3QS801GHcoSsqoQ7zbYq7TUDTp7b%2F%2FRc3ZGo. [Accessed: 10-Jul-2020].
- [42] W. F. Smith, *Princípios de Ciência e Engenharia dos Materiais*, 3^a ed. Lisboa, 1998.
- [43] “Silicone Rubber - Platinum Cure from Smooth-On, Inc.” [Online]. Available: <https://www.smooth-on.com/category/platinum-silicone/>. [Accessed: 24-Jun-2020].
- [44] “Durometer Shore Hardness Scale.” [Online]. Available: <https://www.smooth-on.com/page/durometer-shore-hardness-scale/>. [Accessed: 09-Jun-2020].
- [45] “Flexible 3D Printing Filament – Which Should You Chose? | All3DP.” [Online]. Available: <https://all3dp.com/2/flexible-3d-printing-filament-which-should-you-chose/>. [Accessed: 16-Apr-2020].
- [46] “Section 14: Nonlinear Static Analysis | Inventor Nastran 2018 | Autodesk Knowledge Network.” [Online]. Available: <https://knowledge.autodesk.com/support/inventor-nastran/learn-explore/caas/CloudHelp/cloudhelp/2018/ENU/NINCAD-SelfTraining/files/GUID-156AC319-E5D7-4ED5-9765-4B58D72323D0-htm.html>. [Accessed: 02-Sep-2020].
- [47] SolidWorks, “Understanding Nonlinear Analysis,” *White Pap.*, p. 15, 2010.
- [48] P. A. L. S. Martins, R. M. N. Jorge, and A. J. M. Ferreira, “A comparative study of several material models for prediction of hyperelastic properties: Application to silicone-rubber and soft tissues,” *Strain*, vol. 42, no. 3, pp. 135–147, 2006, doi: 10.1111/j.1475-1305.2006.00257.x.
- [49] Y. Elsayed *et al.*, “Finite Element Analysis and Design Optimization of a Pneumatically Actuating Silicone Module for Robotic Surgery Applications,” *Soft Robot.*, vol. 1, no. 4, pp. 255–262, 2014, doi: 10.1089/soro.2014.0016.
- [50] “Filaflex 70A - 1.75 mm - Recreus Filaflex | Filamento 3d | Impresión 3d.” [Online]. Available: <https://recreus.com/en/filaflex-70a-now-in-1-75-mm/>. [Accessed: 08-Oct-2020].

APPENDIX A (FINGER DIMENSIONS)

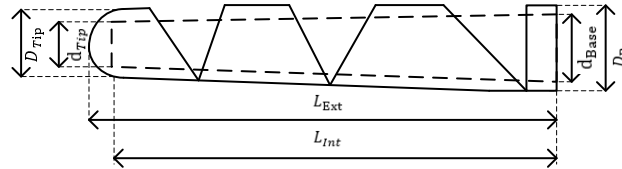


Figure A.1. Nomenclature of dimensions.

Table A.1. Exoskeleton finger dimensions.

Finger	L_{Ext} [mm]	L_{Int} [mm]	D_{Base} [mm]	d_{Base} [mm]	D_{Tip} [mm]	d_{Tip} [mm]
Index	102,5	94,5	20	16	15,5	11,5
Middle	112,5	102,5	20	16	15,5	11,5
Ring	102,5	92,5	20	16	15,5	11,5
Little	87,5	77,5	16	12	12,75	7,75
Thumb	70	62,5	20	16	15,5	7

Note: Only the base and tip diameter values are shown in the table, however the intermediate values are not directly proportional.

Table A.2. Fibre-reinforced actuators dimensions.

Finger	$L_{Int} =$ L_{Ext} actuator [mm]	$d_{Base} =$ D_{Base} actuator [mm]	$d_{tip} =$ D_{Tip} actuator [mm]	Thickness [mm]
Index	94,5	16	11,5	Internal layer – 1,5; PET thread – 0,5 ⁽³⁾ External layer – 1,5 Actuator tip – 4
Middle	102,5	16	11,5	
Ring	92,5	15 ⁽²⁾	10,5 ⁽²⁾	
Little	77,5	11 ⁽²⁾	6,75 ⁽²⁾	
Thumb	62,5	15 ⁽²⁾	6 ⁽²⁾	

Note 1: Only the base and tip diameter values are shown in the table, however the intermediate values are not directly proportional.

Note 2: The diameters of the ring, little and thumb finger are 1 mm smaller than the diameters of the exoskeleton hole.

Note 3: When designing the moulds, it was considered that the diameter thread would be 0,5 mm. However, the thread used was smaller.

APPENDIX B (PRINTING PARAMETERS)


Table B.1. Printing parameters.


Parameters	Finger exoskeleton – Filaflex 82A	Hand exoskeleton – Ninjaxflex	PLA parts
Nozzle temperature	235 °C	240 °C	210 °C
Nozzle size	0.35 mm	0.35 mm	0.35 mm
Printing speed	30 mm/s	20 mm/s	40 mm/s
Infill Pattern	Concentric	Concentric	Grid
Infill Density	100 %	100 %	20 %
Layer height	0.2	0.1	0.2
Adhesion type	Brim	None	* ⁽¹⁾
Flow material	105 %	105 %	100 %
Type of support	None	Touching build plate (70°)	* ⁽²⁾
Retraction	Off	Off	On
Heated bed	None	None	None
* ⁽¹⁾ – Figure 4.6: (b), (c), (d), (e) – Raft; (f), (g), (h) – Brim.			
* ⁽²⁾ – Figure 4.6: (b), (c) – None; (d), (e) – Touching buildplate; (f), (g), (h) – None.			

APPENDIX C (ECOFLEX™ SERIES – TECHNICAL BULLETIN)

Ecoflex™ Series

Super-Soft, Addition Cure Silicone Rubbers





www.smooth-on.com

Cured Material
Certified Skin Safe!

PRODUCT OVERVIEW

Ecoflex™ rubbers are platinum-catalyzed silicones that are versatile and easy to use. Ecoflex™ rubbers are mixed 1A:1B by weight or volume and cured at room temperature with negligible shrinkage. Low viscosity ensures easy mixing and de-airing, or you can choose to mix and dispense using our convenient dispensing cartridges. Cured rubber is very soft, very strong and very "stretchy", stretching many times its original size without tearing and will rebound to its original form without distortion. Ecoflex™ rubbers are water white translucent and can be color pigmented with Silc Pig™ pigments for creating a variety of color effects. You can also add Smooth-On's Silicone Thinner™ to further lower the viscosity. THI-VEX™ silicone thickener can be added by weight to Ecoflex™ silicones for brushable applications.

Soft, Softer, Softest . . . Ecoflex™ rubbers are based on Smooth-On's Dragon Skin™ technology and are currently available in many different hardnesses: Shore A-5, Shore 00-10, 00-20, 00-30 and 00-50. They are suitable for a variety of applications including making prosthetic appliances, cushioning for orthotics and special effects applications (especially in animatronics where repetitive motion is required). Ecoflex™ 5 has a pot life of 1 minute and a demold time of 5 minutes – Available only in dispensing cartridges.

Ecoflex™ 00-33 AF is an **anti-fungal** silicone suitable for making a variety of skin-safe cushioning device configurations that resist fungi for orthopedic and orthotic applications. Cured Ecoflex™ is skin safe and certified by an independent laboratory.

Note: Ecoflex™ 00-10 cures with a "tacky" surface.

TECHNICAL OVERVIEW

	Mixed Viscosity (ASTM D-2393)	Specific Gravity (g/cc) (ASTM D-1473)	Specific Volume (cu. in./lb.) (ASTM D-1475)	Pot Life (ASTM D-2471)	Cure Time	Shore Hardness (ASTM D-2240)	Tensile Strength (ASTM D-412)	100% Modulus (ASTM D-412)	Elongation at Break % (ASTM D-412)	Die B Tear Strength (ASTM D-624)	Shrinkage (in./in.) (ASTM D-2566)
Ecoflex™ 5	13,000 cps	1.07	25.8	1 min.	5 min.	5A	350 psi	15 psi	1000%	75 pli	< .001 in./in.
Ecoflex™ 00-50	8,000 cps	1.07	25.9	18 min.	3 hours	00-50	315 psi	12 psi	980%	50 pli	< .001 in./in.
Ecoflex™ 00-30	3,000 cps	1.07	26.0	45 min.	4 hours	00-30	200 psi	10 psi	900%	38 pli	< .001 in./in.
Ecoflex™ 00-33 AF	3,000 cps	1.07	26.0	45 min.	4 hours	00-33	200 psi	10 psi	900%	38 pli	< .001 in./in.
Ecoflex™ 00-20	3,000 cps	1.07	26.0	30 min.	4 hours	00-20	160 psi	8 psi	845%	30 pli	< .001 in./in.
Ecoflex™ 00-10	14,000 cps	1.04	26.6	30 min.	4 hours	00-10	120 psi	8 psi	800%	22 pli	< .001 in./in.

*All values measured after 7 days at 73°F/23°C

Mix Ratio: 1A:1B by volume or weight	Useful Temperature Range: -65°F to 450°F (-53°C to 232°C)
Color: Translucent	Dielectric Strength (ASTM D-147-97a): >350 volts/mil

PROCESSING RECOMMENDATIONS

PREPARATION... Safety - Use in a properly ventilated area ("room size" ventilation). Wear safety glasses, long sleeves and rubber gloves to minimize contamination risk. Wear vinyl gloves only. Latex gloves will inhibit the cure of the rubber.

Store and use material at room temperature (73°F/23°C). Warmer temperatures will drastically reduce working time and cure time. Storing material at warmer temperatures will also reduce the usable shelf life of unused material. These products have a limited shelf life and should be used as soon as possible. Mixing containers should have straight sides and a flat bottom. Mixing sticks should be flat and stiff with defined edges for scraping the sides and bottom of your mixing container.

Cure Inhibition - Addition-cure silicone rubber may be inhibited by certain contaminants in or on the pattern to be molded resulting in tackiness at the pattern interface or a total lack of cure throughout the mold. Latex, tin-cure silicone, sulfur clays, certain wood surfaces, newly cast polyester, epoxy, tin cure silicone rubber or urethane rubber may cause inhibition. If compatibility between the rubber and the surface is a concern, a small-scale test is recommended. Apply a small amount of rubber onto a non-critical area of the pattern. Inhibition has occurred if the rubber is gummy or uncured after the recommended cure time has passed.

Because no two applications are quite the same, a small test application to determine suitability for your project is recommended if performance of this material is in question.

Safety First!

The Material Safety Data Sheet (MSDS) for this or any Smooth-On product should be read prior to use and is available upon request from Smooth-On. All Smooth-On products are safe to use if directions are read and followed carefully.

Keep Out of Reach of Children

Be careful. Use only with adequate ventilation. Contact with skin and eyes may cause irritation. Flush eyes with water for 15 minutes and seek immediate medical attention. Remove from skin with waterless hand cleaner followed by soap and water.

Important: The information contained in this bulletin is considered accurate. However, no warranty is expressed or implied regarding the accuracy of the data, the results to be obtained from the use thereof, or that any such use will not infringe upon a patent. User shall determine the suitability of the product for the intended application and assume all risk and liability whatsoever in connection therewith.

To prevent inhibition, one or more coatings of a clear acrylic lacquer applied to the model surface is usually effective. Allow any sealer to thoroughly dry before applying rubber. Note: Even with a sealer, platinum silicones will not work with modeling clays containing heavy amounts of sulfur. Do a small scale test for compatibility before using on your project.

Applying A Release Agent - Although not usually necessary, a release agent will make demolding easier when pouring into or over most surfaces. Ease Release™ 200 is a proven release agent for use with silicone rubber. Mann Ease Release™ products are available from Smooth-On or your Smooth-On distributor.

IMPORTANT: To ensure thorough coverage, lightly brush the release agent with a soft brush over all surfaces of the model. Follow with a light mist coating and let the release agent dry for 30 minutes.

If there is any question about the effectiveness of a sealer/release agent combination, a small-scale test should be made on an identical surface for trial.

MEASURING & MIXING...

Stir Part A and Part B thoroughly before dispensing. After dispensing required amounts of Parts A and B into mixing container (1A:1B by volume or weight), mix thoroughly for 3 minutes making sure that you scrape the sides and bottom of the mixing container several times. After mixing parts A and B, vacuum degassing is recommended to eliminate any entrapped air. Vacuum material for 2-3 minutes (29 inches of mercury), making sure that you leave enough room in container for product volume expansion.

POURING, CURING & MOLD PERFORMANCE...

For best results, pour your mixture in a single spot at the lowest point of the containment field. Let the rubber seek its level up and over the model. A uniform flow will help minimize entrapped air. The liquid rubber should level off at least 1/2" (1.3 cm) over the highest point of the model surface.

Curing / Post Curing - Allow rubber to cure as prescribed at room temperature (73°F/23°C) before demolding. Do not cure rubber where temperature is less than 65°F/18°C. Optional: Post curing the mold will aid in quickly attaining maximum physical and performance properties. After curing at room temperature, expose the rubber to 176°F/80°C for 2 hours and 212°F/100°C for one hour. Allow mold to cool to room temperature before using.

If Using As A Mold - When first cast, silicone rubber molds exhibit natural release characteristics. Depending on what is being cast into the mold, mold lubricity may be depleted over time and parts will begin to stick. No release agent is necessary when casting wax or gypsum. Applying a release agent such as Ease Release™ 200 (available from Smooth-On) prior to casting polyurethane, polyester and epoxy resins is recommended to prevent mold degradation.

Thickening Ecoflex™ Silicones - THI-VEX™ is made especially for thickening Smooth-On's silicones for vertical surface application (making brush-on molds). Different viscosities can be attained by varying the amount of THI-VEX™. See the THI-VEX™ technical bulletin (available from Smooth-On or your Smooth-On distributor) for full details.

Thinning Ecoflex™ Silicones - Smooth-On's Silicone Thinner™ will lower the viscosity of Ecoflex™ silicones for easier pouring and vacuum degassing. A disadvantage is that ultimate tear and tensile are reduced in proportion to the amount of Silicone Thinner™ added. **It is not recommended to exceed 10% by weight of total system (A+B).** See the Silicone Thinner™ technical bulletin (available from Smooth-On or your Smooth-On distributor) for full details.

Mold Performance & Storage - The physical life of the mold depends on how you use it (materials cast, frequency, etc.). Casting abrasive materials such as concrete can quickly erode mold detail, while casting non-abrasive materials (wax) will not affect mold detail. Before storing, the mold should be cleaned with a soap solution and wiped fully dry. Two part (or more) molds should be assembled. Molds should be stored on a level surface in a cool, dry environment.



Call Us Anytime With Questions About Your Application.

Toll-free: (800) 381-1733 Fax: (610) 252-6200

The new www.smooth-on.com is loaded with information about mold making, casting and more.

122018-JR

APPENDIX D (FILAFLEX 82A – TECHNICAL BULLETIN)



TECHNICAL DATA SHEET

FILAFLEX 82A ORIGINAL

Description

Filaflex is a Thermoplastic Polyether-Polyurethane elastomer with additives that allow high printability in FDM printers. Filaflex® has a remarkable hydrolysis resistance, high resistance to bacteria and low temperature flexibility properties in printed parts.

Physical properties	Value	Unit	Test method according to
Material density	1.12	g/cm ³	DIN EN ISO 1183-1 A

Mechanical properties	Value	Unit	Test method according to
Hardness	82	Shore A	DIN ISO 7619-1 (35)
Hardness (approx. 45)	31	Shore D	DIN ISO 7619-1 (35)
Tensile strength	45	MPa	DIN 53504-52
Elongation at break	600	%	DIN 53504-52
Stress at 20% elongation	2.5	MPa	DIN 53504-52
Stress at 100% elongation	6	MPa	DIN 53504-52
Stress at 300% elongation	10	MPa	DIN 53504-52
Tear strength	70	N/mm	DIN ISO 347-1 (b)
Abrasion loss	25	mm ³	DIN ISO 4643-A
Compression set: 25°C / 72 hours	25	%	DIN ISO 815
Compression set: 70°C / 24 hours	45	%	DIN ISO 815
Tensile strength after storage in water at 80°C for 42 days	32	MPa	DIN 53504-52
Elongation at break after storage in water at 80°C for 42 days	800	%	DIN 53504-52
Notched impact strength (Charpy) at 125°C	nb	kJ/m ²	DIN EN ISO 179-1
Notched impact strength (Charpy) at -30°C	nb	kJ/m ²	DIN EN ISO 179-1

Printing properties	Recommended
Printing temperatures	215 - 250°C
Printing speed	20 - 50 mm/s
Hot-bed temperature	0°C
Optimal layer height	0.2 mm
Minimal nozzle diameter	0.4 mm or higher
Retraction parameters	3.5 - 6.5 mm (speed 20 - 160 mm/s)

RECREUS INDUSTRIES S.L. VAT: ESB54876479
C/El Envelope, F13-F14, Pol. Ind. Finca Lacy
03600, Elda (Alicante) - SPAIN

(0034) 865 777 966
info@recreus.com
www.recreus.com

RECREUS INDUSTRIES S.L. Safety Data sheet according to Regulation (EC) No. 1907/2006 as amended from time to time.
Date / Revised: 18/04/2018
Product: Filaflex 82A Original

APPENDIX E (NINJAFLEX – TECHNICAL BULLETIN)



NinjaFlex® 3D Printing Filament

Flexible Polyurethane Material for FDM Printers

NinjaFlex flexible filament leads the industry with superior flexibility and longevity compared to non-polyurethane materials. Its consistency in diameter and ovality (roundness) outpaces other polyurethane materials. Made from a specially formulated thermoplastic polyurethane (TPU) material, this patented technology contains a low-tack, easy-to-feed texture. The result is uniquely flexible, strong prints ideal for direct-drive extruders.

General Properties	Test Method	Imperial	Metric
Specific Gravity	ASTM D792	1.19 g/cc	1.19 g/cc
Moisture Absorption - 24 hours	ASTM D570	0.22 %	0.22 %
Mechanical Properties			
Tensile Strength, Yield	ASTM D638	580 psi	4 Mpa
Tensile Strength, Ultimate	ASTM D638	3,700 psi	26 Mpa
Tensile Modulus	ASTM D638	1,800 psi	12 Mpa
Elongation at Yield	ASTM D638	65%	65%
Elongation at Break	ASTM D638	660%	660%
Toughness (integrated stress-strain curve; calculated stress x strain)	ASTM D638	12,000 in-lbF/in ³	82.7 m ³ N/m ³ x10 ⁴
Hardness	ASTM D2240	85 Shore A	85 Shore A
Impact Strength (notched Izod, 23C)	ASTM D256	2.0 ft-lb/in ²	4.2 kJ/m ²
Abrasion Resistance (mass loss, 10,000 cycles)	ASTM D4060	0.08 g	0.08 g
Thermal Properties			
Melting Point (via Differential Scanning Calorimeter)	DSC	420° F	216° C
Glass Transition (Tg)	DSC	-31° F	-35° C
Heat Deflection Temperature (HDT) @ 10.75psi/ 0.07 MPa	ASTM D648	140° F	60° C
Heat Deflection Temperature (HDT) @ 66psi/ 0.45 MPa	ASTM D648	111° F	44° C

NinjaFlex filament is capable of being printed by a variety of printers in a variety of configurations. This specification sheet gives results as they pertain to the defined test standard and specimen details. Different slicing and/or printing configurations, test conditions, ambient environments, etc. may result in different results.

Impact Strength and Heat Deflection Temperature results were both provided by an accredited university testing laboratory. Specific Gravity and Hardness are innate characteristics of the material. Moisture Absorption, values associated with the Tensile Strength tests, Melting Point and Glass Transition data were prepared by Fenner Drees, Inc.

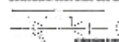
NinjaTek makes no warranties of any type, express or implied, including, but not limited to, the warranties of fitness for a particular application.

Test Specimen Details (by ASTM Test Number)
All printed specimens were created using the TACS printer 0.75mm nozzle. For ASTM D638 tests, the extrusion multiplier is 1.05.

Specific Gravity (D792): Results determined by nature of material.

Moisture (D570): 3g of filament tested in moisture analyzer evaluated at 125°C until the mass change is + 0.005% over 1 minute.

Tensile (D638): Dogbone Style IV, 100% RH, diagonal line 90°. Dimensions: See block. See drawing for other dimensions.



Hardness (D2240): Solid testing block.



Impact (D256): Un-notched test specimen, notch added post print by testing facility.



Abrasion (D4060): Rectangular block sized to fit labor abrasion.



HDT (D648): Bar shape.

